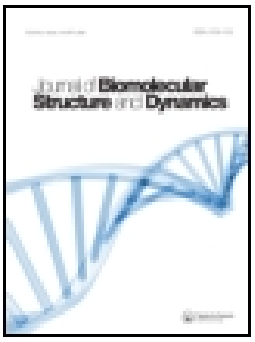

Journal of Biomolecular Structure and Dynamics

ISSN: 0739-1102 (Print) 1538-0254 (Online) Journal homepage: http://www.tandfonline.com/loi/tbsd20

Ligand and structure based in silico studies to identify kinesin spindle protein (KSP) inhibitors as potential anticancer agents

Chandrasekaran Balakumar, Muthusamy Ramesh, Chuin Lean Tham, Samukelisiwe Pretty Khathi, Frank Kozielski, Cherukupalli Srinivasulu, Girish A. Hampannavar, Nisar Sayyad, Mahmoud E. Soliman & Rajshekhar Karpoormath

To cite this article: Chandrasekaran Balakumar, Muthusamy Ramesh, Chuin Lean Tham, Samukelisiwe Pretty Khathi, Frank Kozielski, Cherukupalli Srinivasulu, Girish A. Hampannavar, Nisar Sayyad, Mahmoud E. Soliman & Rajshekhar Karpoormath (2017): Ligand and structure based in silico studies to identify kinesin spindle protein (KSP) inhibitors as potential anticancer agents, Journal of Biomolecular Structure and Dynamics, DOI: 10.1080/07391102.2017.1396255

To link to this article: http://dx.doi.org/10.1080/07391102.2017.1396255

Accepted author version posted online: 24 Oct 2017.

Submit your article to this journal

Article views: 16

View related articles

View Crossmark data

Full Terms & Conditions of access and use can be found at
http://www.tandfonline.com/action/journalInformation?journalCode=tbsd20

Download by: [UCL Library Services] **Date:** 09 November 2017, At: 08:22

Publisher: Taylor & Francis
Journal: *Journal of Biomolecular Structure and Dynamics*
DOI: http://doi.org/10.1080/07391102.2017.1396255

Check for updates

Ligand and structure based *in silico* studies to identify kinesin spindle protein (KSP) inhibitors as potential anticancer agents

ChandrasekaranBalakumar,[a] MuthusamyRamesh,[a] Chuin Lean Tham,[b] Samukelisiwe Pretty Khathi,[a] Frank Kozielski,[b] CherukupalliSrinivasulu,[a] Girish A. Hampannavar,[a] NisarSayyad,[a] Mahmoud E. Soliman,[a] and Rajshekhar Karpoormath[a]*

[a] *Discipline of Pharmaceutical Sciences, College of Health Sciences, University of KwaZulu-Natal (UKZN), Westville, Durban 4001, South Africa.*

[b] *Department of Pharmaceutical and Biological Chemistry, The School of Pharmacy, University College London, 29-39 Brunswick Square, London WC1N 1AX, U.K.*

*Corresponding author: karpoormath@ukzn.ac.za **(**R. Karpoormath)

Abstract

Kinesin spindle protein (KSP) belongs to the kinesin superfamily of microtubule-based motor proteins. KSPis responsible for the establishment of the bipolar mitotic spindle which mediates cell division. Inhibition of KSP expedites the blockade of the normal cell cycle during mitosis throughthe generation of monoastralMTarrays that finally cause apoptotic cell death. As KSP is highly expressed in proliferating/cancer cells, it has gained considerable attention as a potential drug target for cancer chemotherapy. Therefore, this study envisaged to design novel KSP inhibitors by employing computational techniques/tools such as pharmacophore modeling, virtual database screening, molecular docking, and molecular dynamics. Initially, the pharmacophore models were generated from the dataset of highly potent KSP inhibitors and the pharmacophore models were validated against *in house*test set ligands.The validated pharmacophore model was then taken for database screening (Maybridgeand ChemBridge) to yield hits, which were further filtered for their drug-likeliness. The potential hits retrieved from virtual database screening were docked using CDOCKER to identify the ligandbinding landscape. The top-ranked hits obtained from molecular docking were progressed to molecular dynamics (AMBER) simulations to deduce the ligand binding affinity. This study identified MB-41570 and CB-10358 as potentialhits and evaluated experimentally using *in vitro*KSP ATPase inhibition assays.

Key words: KSP inhibitors; pharmacophore modeling;CDOCKER; molecular dynamics; KSP ATPase enzyme inhibition.

List of abbreviations

ADP	adenosine diphosphate
AMBER	assisted model building with energy refinement
ATP	adenosine triphosphate
CB	chembridge
CG	conjugate gradient
DS	discovery studio
GI	gastro intestinal
GAFF	generalized amber force field
KSP	kinesin spindle protein
MB	maybridge
MT	microtubule
MD	molecular dynamics
MM/GBSA	molecular mechanics/generalized Born and surface area continuum solvation
PDB	protein data bank
RoG	radius of gyration
RMSD	root mean square deviation
RMSF	root mean square fluctuations
SD	steepest descent

3D	three dimensional
vdW	van der Waals

Introduction

Kinesins are microtubule (MT) based motor proteins that belong to the kinesin superfamily. In mitotic cells, they are involved in various key cellular events such as mitotic spindle assembly, re-modeling of MTs, the positioning of subcellular organelles, and chromosome segregation(Hirokawa, 1998).Kinesin spindle protein (also known as KSP, Eg5 or KIF11) is a plus-end-directed N-terminal MT motor and is responsible for the establishment of the bipolar organization of the mitotic spindle(Goodson, Kang, & Endow, 1994).The mitotic spindle segregates chromosome to process through mitosis. If a functional spindle fails to form, normal segregation of chromosomes does not take place.Consequently,checkpoint proteins inhibit cell division resulting in mitotic arrest (DeBonis et al., 2003) followed by cell death.KSP is highly expressed in proliferating human tissues and tumors of the colon, breast, uterus, ovary,and lungs(Compton, 2000).Therefore, KSP is a potential drug target in cancer chemotherapy. Inhibitors of KSP are mitosis-specific that preferably act on cells undergoing cell division(Sarli & Giannis, 2008).Hence,KSP inhibitorsmay likely to have fewer side effects (with the exception of neutropeniaa main side effect) while comparing with other agents affecting MT-based processes (Sakowicz et al., 2004; Song, Zhou, Wang, & Li, 2013).

The KSP inhibitorsare structurally diverse and include (i) six-membered fused heterocycles (CK-0106023,monastrol, and dimethylenastron), (ii) five-membered nitrogen-containing heterocycles(dihydro-pyrazolothiophenes, dihydro-thiadiazoles,and thiazoles), (iii)biaryl compounds (GSK-1 and GSK-2) and (iv)natural products (adociasulfate-2)(El-Nassan, 2013). Few of the KSP inhibitors were studied under different stages of clinical trials.

SB-743921, a chromen-4-one derivative was evaluated in clinical trials(phase-II) to treat non-Hodgkin lymphoma and Hodgkin lymphoma(https://clinicaltrials.gov).Further, it has demonstrated 5-fold more potency than ispinesib in cell-based assays (Holen et al., 2011; Yin et al., 2015).ARQ-621 is an allosteric inhibitor evaluated against solid metastatic tumours and hematologic malignancies in a phase-Istudy (https://clinicaltrials.gov). Similarly, AZD-4877 was evaluated under phase-II clinical trial for the treatment of advanced bladder cancer (https://clinicaltrials.gov). A pyrrole analogue, MK-0711 was studied in patients with advanced solid tumours under phase-I clinical trial (https://clinicaltrials.gov). Filanesib (also known as ARRY-520) is now under phase-III clinical studies in the management of multiple myeloma in combination with carfilzomib (https://clinicaltrials.gov)(Figure 1). Ispinesib (SB-715992) was investigated in phase-II studies in treating patients with metastatic or unresectable kidney cancer (https://clinicaltrials.gov) (Figure 2). Similarly, litronesib(known as LY2523355) is an ATP non-competitive, and allosteric inhibitor evaluated in patients with breast cancer (phase-II) (https://clinicaltrials.gov) and reported as a promising anticancer agent (Wakui et al., 2014)(Figure 2).

KSP encompasses 1057 amino acid residues and is divided into three major domains namely the motor domain (N-terminal), stalk and tail (C-terminal) domains (Figure 3). A short stretch of initial 20 amino acids precedes the motor domain (21-356 amino acids) followed by a neck linker (357-363),the internal stalk responsible for oligomerisationand the C-terminal tail (364-1057),which includes a phosphorylation-site (Thr927 in human KSP)(Blangy, Arnaud, & Nigg, 1997; Turner et al., 2001).The motor domain is the highly significant segment as it is responsible for the hydrolysis of adenosine triphosphate (ATP) to adenosine diphosphate (ADP) thus generating the required energy for movement of the motor along MTs.KSP utilizes the energy to propel spindle MTs in an antiparallel manner through its motor activity and sliding them apart. Thus, it contributes to the separation of centrosomes and the generation of bipolar spindle assembly during cell division(Civelekoglu-Scholey & Scholey, 2010; Saunders, Powers, Strome, & Saxton, 2007; Wordeman, 2010).As the motor domain of KSP plays a central role in cell division, many research groups determined the structure of the motor domain and studied the mode of action of small organic moleculesas KSP inhibitors(Barsanti et al., 2010; Fraley et al., 2006; Kaan, Ulaganathan, Rath, et al., 2010; Kaan, Ulaganathan, Hackney, & Kozielski, 2010; Wang et al., 2012). Recently, the X-ray crystal structure of the KSP motor domain in complex with SB-743921 a second generation ispinesib analogue and ADP was reported in the protein data bank (PDB ID: 4BXN)(Figure 4). The inhibitor was found to bind at the allosteric binding-siteformed by helix α2/loop L5/α3(Talapatra, Anthony, Mackay, & Kozielski, 2013).

Computational methods such as ligand-based (pharmacophore model and 3D QSAR), structure-based (molecular docking or molecular dynamics simulations) and integrated approaches are generally employed in designing therapeutically active new chemical entities.

These approaches have been employed successfully to discover drugs such as dorzolamide (carbonic anhydrase inhibitor), captopril (angiotensin-converting enzyme inhibitor), saquinavir, ritonavir, indinavir and raltegravir (anti-HIV drugs) and tirofiban (fibrinogen antagonist)(Gu, Zhang, & Yuan, 2014; Hartman et al., 1992; Talele, Khedkar, & Rigby, 2010; Vijayakrishnan, 2009)as well as drug metabolism profiles(Ramesh & Bharatam, 2014). First,a quantitative 3D pharmacophore model with good correlation coefficient (r = 0.965) for KSP inhibitors was developed by Liu and co-workers. The studyreportedthe best hypothesis bearing four different chemical features (ring aromatic, hydrogen bond acceptor, hydrogen bond donor, and hydrophobic) using HypoGenmodule implemented in Catalyst software(Liu, You, & Chen, 2007). Subsequently, Jiangand his colleagues reported docking (structure-based) studies of 15 KSP inhibitors and proposed the significance of a ‘minor pocket’ that is situated away from the ‘main pocket’ in enhancing the binding affinity of ligands(Jiang, Chen, Wang, & You, 2007).

Till date, there are49 solved X-ray crystal structures ofKSP available in the PDB(http://www.rcsb.org/pdb/).Thus, these structures paved a way towards the determination of novel KSP inhibitors using structure-based drug design method. In 2012, Nagarajan and collaborators reported combined ligand- and structure-based virtual screening approaches toidentify novel KSP inhibitors. In their study, the interaction-based pharmacophore models (IBPs) were developed and validated using six different complexes of KSP crystal structures. The generated models were appliedto filter the ChemDiv database (0.7 million) to identifyinitial hits. The IBP-based hits were subjected to docking (GOLD and GLIDE),biological screening (inhibition of tumor cell proliferation and basal Eg5 ATPase activity),and phenotypic analysis. These integrative approaches identified substituted imidazolidinecompound as a novel KSP inhibitor(Nagarajan, Skoufias, Kozielski, & Pae, 2012)(**9**,Figure5). Similarly, Carbajales and co-workers analyzedKSP allosteric binding-sitefrom the 24 crystal structures of allostericinhibitor complexesand developed planar heterocycles based on the crystal structures of KSP (PDB ID: 2GM1). This structure-guided design led to the discovery of benzimidazole-based KSP inhibitors throughmulticomponent synthesis(**10**and **11**, Figure 5)(Carbajales et al., 2014).Recently (2015), Yokoyama and co-workers reported the crystal structure (PDB ID: 4WPN) and biochemical characterisation of the Eg5 motor domain in complexwith a new type of allosteric inhibitor (PVZB-1194). This biphenyl-type inhibitor was proposed to bind within the novel α4/α6 allosteric pocket, whereas residues in the allosteric pocket formed by α2/loop L5/α3 are responsible for the binding of conventional KSP inhibitors (Yokoyama et al., 2015).In recent literature reports

(2016), chemical feature-based pharmacophore modelswere generated and validated. Subsequently, the best validated model was considered for virtual screening including the drug-like parameters to yield hits. Based on molecular interactions (docking) and computed electronic parameters (density functional theory calculations), authors reported six lead compounds as novel KSP inhibitors(Karunagaran, Subhashchandrabose, Lee, & Meganathan, 2016).

Currently, there are no specific KSP inhibitor drugs in the market. However, few KSP inhibitors (Figure 1 and 2) are at different stages of clinical trials. This prompts medicinal chemists to design and develop new KSP inhibitors through rational drug discovery approaches. Therefore, in the present study, we envisaged to develop novel KSP inhibitors by employing ligand- and structure-based drug design techniques. In addition, *in vitro* enzyme assay evaluations were carried out for the identified hits against the basal and MT-stimulated ATPase activity of KSP.

2. Materials and methods

2.1. Collection of training and test set

The selection of a suitable training set is crucialfor the generation of ligand-based pharmacophore models. Additionally, it is necessary to consider an appropriate test set of ligands that are not employed for the generation of models but may assistin the validation of the obtained pharmacophore models. In this study, a data set of highly active KSP inhibitors incorporating clinical/preclinical trial molecules (Cox et al., 2008; Gerecitano et al., 2009; Roecker et al., 2007; Rosen et al., 2010; Theoclitou et al., 2011; Woessner et al., 2009)as a training set (Figure1). Further, it was taken into an account that the selected ligands were pharmacologically screened under similar experimental conditions (*in vitro*), and structural diversity. Many of the reported active and inactive KSP inhibitors exhibited a stereocenter in their chemicalstructure. Hence,appropriate stereochemistry of ligands was carefully considered in the training as well as the test sets.

2.2. Generation of pharmacophore models

Pharmacophore modeling relates pharmacological activity with the 3D spatial arrangement of various chemical features in a set of active molecules.HipHop is a well-known application for common feature-based pharmacophore model generation. It is incorporated in Discovery Studio (DS) software package as ‘Common Feature

PharmacophoreGeneration' protocol(DassaultSystèmes BIOVIA, Discovery Studio Modeling Environment, Release 4.5, San Diego: DassaultSystèmes, 2015).The present study includes the six most active ligands in the training set to build/construct suitablepharmacophore models.To generate the pharmacophore models, aconformational analysis was carried out for all molecules of thetraining set using the same software package. These conformations were generated by a fast conformational method with a maximum limit of 255,having an energy 20 kcal/molhigher than the global energy minimum(Neves, Dinis, Colombo, & Sá e Melo, 2009). Based on the presence of certain chemical features in the training set, hydrogen bond acceptor (A), hydrogen bond donor (D), hydrophobic (H), hydrophobic aliphatic (HY-Ali), positively ionizable (P) and ring aromatic (R) chemical functions were considered for feature analyses. The minimum inter-feature distance was set to the default value (2.97 Å).

2.3. Validation of pharmacophore model

The pharmacophore model usually consists of certain fixed parameters/filters that every new chemical entity has to satisfy inorder to be considered as an active inhibitor. The validation of pharmacophore model is performed by screening an *in house* test set consisting of both known active and inactive molecules. This is an indispensable step for the validation of the pharmacophore model. The test set was thoroughly verified to exclude high molecular weight compounds, prodrugs, and peptides. The *in house* test set constituted of 54 active KSP inhibitors (IC_{50} = 0.1-100.0 nM) and 755 inactive molecules (IC_{50} >100.0 nM). From the 54 active KSP inhibitors, 36 ligands were identified as 'highly active' (IC_{50} values < 20 nM) while the remaining 18 ligands were arbitrarily classified as 'moderately active' (IC_{50} = 20 to 100 nM). Although, from the pharmacological point of view the ligands with IC_{50} values 100 to 500 nM are also considered as active inhibitors, however in our study the cut off IC_{50} value was set at 100 nM as one of the crucial parameter to identify highly potent inhibitors (Supplementary Table S1).

2.4. Virtual screening

Virtual 3D database screening can offer a valuable route to identify potential lead molecules for further drug development.Eventually, database searchprovides an advantage that theidentified or retrieved molecules can be procured handily or synthesized conveniently for pharmacological screeningprotocols when compared to other *de novo*drug design methodologies(Michaux et al., 2006).The approach uses 3D features of the pharmacophore model asa query in the database screening to discover novelhit molecules. Twodatabase search methods (i) Fast/Flexible (diverse low-energy conformation) and Best/Flexible(best coverage of conformational space)are incorporated in DS. In general, Best/Flexible search method is employed for virtual database screening to obtain better results (Karunagaran, Subhashchandrabose, Lee, & Meganathan, 2016)and the same method was implemented in our study. Two different databases, namely Maybridge-HitDiscover (MB)and ChemBridge (CB) were searched to identify potential KSP targeting hits. Further, the molecules were filtered fortheir drug-like properties using Lipinski's rule of five[molecular weight less than 500, less than 5 hydrogen bond donor groups, less than 10 hydrogen bond acceptor groups and an octanol/water partition co-efficient (LogP) value of less than 5], Veber rule [10 or less than 10 rotatable bonds and polar surface area equal to or less than 140 Å^2](Veber et al., 2002)andADMET (Absorption, Distribution, Metabolism, Excretion, andToxicity) filters using DS. Hit ligands which qualified for all of thesescreening protocols were takenforwardfor molecular docking studies.

2.5. Molecular docking

Molecular docking is a structure-based *in silico* approach to identify the possible ligand binding landscape inside the binding-site of a macromolecular protein/receptor. Molecular docking was conducted using the CDOCKER module under the receptor-ligandinteractions protocol implemented in DS. It is a grid-based docking method thatemploys CHARMm force field. In this protocol, a macromolecule is kept under constraint while ligands are enabled for their conformational flexibility during the refinement step. A high-temperature molecular dynamics (MD) pursued by random rotations resulted in different conformations for initial ligand structure. The final refinement of random conformations was implemented through a grid-based simulated annealingfollowed by either grid-based or full forcefield minimization(Wu, Robertson, Brooks, & Vieth, 2003).To perform molecular docking,a crystal structure of humanKSP with bound inhibitor (SB-743921) was used (PDB ID: 4BXN)(Talapatra et al., 2013).Prior to the molecular docking, KSPwas prepared using 'prepare protein' implemented under 'Macromolecules' module of DS. All the water molecules, chloride ions, and cadmium ions present in co-crystallized structure ofthe protein were removed and the missing hydrogen atoms were added to the KSP structure (Figure 6A).The co-factor (ADP)present in the crystal structure was retained for moleculardocking protocol in which the pH for protonation was set at 7.4. To optimize the molecular docking protocol, several docking runs were performed. During the optimization, various parameters were set for theactive-site radius (15Å), scoring function (CDOCKER energy), algorithm (CDOCKER), physiological state of the ligands (ionized state), root mean square deviation (< 1.5) to enhance the docking accuracy. By employing receptor-ligand interactions tool, the total protein was defined as a receptor and a binding-site sphere was generated with the radius of 15Å around the inhibitory ligand present in the protein structure (Figure 6B).

Further, the ligands were prepared for ionization change, Lipinski's filter, and 3D conformation generation. For the purpose of the validation of the molecular docking protocol, the bound ligand (SB-743921) was extracted from the co-crystallized complex and was docked into the definedbinding-site of the protein. Similarly, molecules present in the training set, test set and the hits retrieved from virtualscreeningwere also docked into the pre-defined binding-site of KSP (target protein) with default settings of DS. After completion of docking, the protein-ligand complexes were analyzed to investigate the type of interactions and CDOCKER energy values(Yang, Yang, Zou, Li, & Zhu, 2016).The final hits of molecular docking were selected based on their higher (most negative, thus favourable to binding)CDOCKER energy and selected complexes were subjected to molecular dynamics simulations.

2.6. Molecular dynamics

Molecular dynamics (MD) is a widely used structured-based *in silico* approach to determine the binding efficiency of ligands inside the binding-site of macromolecules(Zhao & Caflisch, 2015). All MD simulations were run in AMBER 14.0 software package in SANDER(Case et al.,2014).The protein-ligand complexes of 4BXN-SB743921 (native ligand in the crystal structure)(Talapatra et al., 2013) and the top-ranked hit molecules of molecular dockingfrom each database weresubjected to MD simulations. The ligand binding pose obtained from top-ranked molecular docking was considered as starting point to runMD simulations. Initially, the geometry of the protein and bound ligands from the docked complexes were separated using Chimera Software package(Pettersen et al., 2004).The ligands were defined with Generalized Amber Force Field (GAFF) and the partial atomic charges were derived from AM1-BCC method of Antechamber. The protein was defined with

AMBER99SB force field and was prepared in Leap module to add missing hydrogen and to generate the parameters for a solvated protein-ligand complex(Kholmurodov, Smith, Yasuoka, Darden, & Ebisuzaki, 2000).The complex was enclosed with TIP3P water molecules in a box which was extended up to 10 Å from the center of the molecule(Jorgensen, Chandrasekhar, Madura, Impey, & Klein, 1983). The solvated complex was electro-neutralized with counter ion Na^+. Four Na^+ions were added to neutralize the system.To remove the bad contacts, partial minimization was carried out with a restraint potential of 500 kcal $mol^{-1}Å^{-2}$. Partial minimization was run for 1000 steps of steepest descent (SD) followed by 500 steps of conjugate gradient (CG). Further, the complex was energetically minimized using 50 steps of SD followed by 150 steps of CG. After minimization, heating was conducted graduallyfrom 0 to 300 K for 5 psusing LangevinDynamics. Then the system was equilibrated at 300 K in a constant pressure and temperature ensemble for 500 ps. The pressure of the system was maintained at 1 bar using Berendsenbarostat. All the bonds involving hydrogens were constrained using SHAKEalgorithm(Ryckaert, Ciccotti, & Berendsen, 1977).MD was run without restrain at a temperature of 300 K and a pressure of 1 bar. A5 ns MD was run with a time step of 2fs and a distance cutoff of 12.0 Å for the non-bonded interactions(Berendsen, Postma, van Gunsteren, DiNola, & Haak, 1984).The trajectories were saved and analyzed for every 1 ps. Visualization of trajectories was carried out using Chimera software package. After MD simulations, binding free energies were computed.

2.7. MM/GBSA and other post dynamics analyses

Binding free energies were defined as bound and unbound states of protein-ligand complexes.After 5ns of MD simulation, the binding free energies were computed by MM/GBSA method[Eqn 1-5](Hou, Wang, Li, & Wang, 2011; Lyne, Lamb, & Saeh, 2006).Binding affinities were estimated by averaging snapshots taken from the MD trajectories. The binding free energies were averaged over 1000 snapshots of MD trajectories.

$\Delta G_{bind} = G_{complex} – G_{receptor} - G_{ligand}$.. (1)

$\Delta G_{bind} = E_{gas} + G_{sol} – TS$...(2)

$E_{gas} = E_{int} + E_{vdw} + E_{ele}$..(3)

$G_{sol} = G_{GB} + G_{SA}$...(4)

$G_{SA} = {}_{\Upsilon}SASA$...(5)

E_{gas}: gas-phase energy that consists of the internal energy(E_{int}), coulomb energy (E_{ele}), and thevan der Waals energies (E_{vdW}).E_{gas} was directly estimatedfrom the FF99SB force field terms.The solvationfreeenergy (G_{sol}) was estimated from the energy contributionfrom the polar states (G_{GB}) and nonpolar states (G_{SA}). Thenonpolar solvation energy(G_{SA}) was determined from theSASA using a water probe radius of 1.4 Å, whereasthe polar solvation (G_{GB}) contribution was estimated bysolving the GB equation.The total entropy of the soluteand temperature was denoted by S and T, respectively.Post-MD analyses (root mean square deviation, root mean square fluctuation, and radius of gyration), the snapshot of the structures during simulation and average structure were carried out using CPPTRAJ and PTRAJ module of AMBER 14(Roe & Cheatham, 2013; Duan, Liu, & Zhang, 2016).

2.8. Chemical Synthesis and Characterization

2.8.1. General

Melting points of all the synthesized compounds were recorded in open capillaries using Electro-thermal (IA9300) digital melting point apparatus and are uncorrected. A Bruker FT-IR spectrophotometer with universal ATR sampling accessory was used to record all IR spectra. ^{1}H and ^{13}C NMR spectra were recorded on NMR spectrometer (Bruker Avance IV) at 400 and 101 MHz, using $CDCl_3$with TMS as an internal standard and reported in parts per million (ppm). The progress of the reactions and the purity of the synthesized compounds were monitored by Thin Layer Chromatography (TLC) on precoated silica gel 60 F_{254} (mesh) (E. Merck) and spots were visualized under UV light (long and short wavelength). The analytical grade (AR) chemicals and reagents were obtained from Merck and Sigma-Aldrich and were used as such without any further purification.The ChemBridge ligand (CB-10358) was procured directly from ChemBridge Corporation, San Diego, USA.

2.8.2. Synthesis of diethyl 2-amino-4,7-dihydrothieno[2,3-c]pyridine-3,6(5H)-dicarboxylate (3)

Ethyl 4-oxo-piperidine-1-carboxylate **1** (0.04 mol; 6.0 ml), ethyl cyano acetate **2** (0.04 mol; 4.52 ml), powdered sulphur (0.04 mol; 1.28 gm), and absolute ethanol (40 ml) were taken in a conical flask and warmed at 50-60 °C. Then diethylamine (4 ml) was added dropwise with constant stirring until all sulphur went into solution. The stirring was continued for an additional one hour until brownish-yellow coloured solid separated, then it was cooled to room temperature and filtered. The crude product was dried and recrystallized from ethanol to yield pure diethyl 2-amino-4,7-dihydrothieno[2,3-*c*]pyridine-3,6(5*H*)-

dicarboxylate (**3**).

Brownish-yellow solid, yield: 9.1 gm (87%), mp: 160-162 °C; IR (KBr): 3422, 3318 (NH_2), 1685 (ester-C=O), 1665 (piperidine-C=O) cm^{-1}; ^1H NMR (400 MHz, $CDCl_3$): δ 1.24-1.29 (t, J = 7.02 Hz, 3H, $CH_2C\underline{H}_3$), 1.30-1.35 (t, J = 7.10 Hz, 3H, $CH_2C\underline{H}_3$), 2.80 (s, 2H, CH_2, piperidine), 3.64 (s, 2H, CH_2, piperidine), 4.12-4.18 (q, J = 7.06 Hz, 2H, $C\underline{H}_2CH_3$), 4.21-4.27 (q, J = 7.13 Hz, 2H, $C\underline{H}_2CH_3$), 4.38 (s, 2H, CH_2, piperidine), 5.5 (br s, 2H, NH_2) ppm; ^{13}C NMR (100 MHz, $CDCl_3$, CPD): δ 14.58, 14.86, 27.22, 41.44, 42.78, 59.78, 61.71, 155.71, 162.51, 165.94 ppm.

2.8.3. Synthesis of diethyl 2-(2-chloroacetamido)-4,7-dihydrothieno[2,3-c]pyridine-3,6(5H)-dicarboxylate (4)

The compound **3** (0.02 mol; 5.967 gm) was dissolved in dry *N,N*-dimethyl formamide (40 ml) and added triethylamine (0.02 mol; 2.8 ml) followed by the addition of a solution of chloroacetyl chloride (0.024 mol; 1.9 ml) in DMF (10 ml) slowly dropwise. The reaction mixture was stirred at room temperature for additional two hours until all starting material converted to product (monitored by TLC). Then the mixture was kept at room temperature to precipitate dark coloured solids. The product was isolated by filtration under vacuum, dried and recrystallized with absolute alcohol to obtain pure intermediate **4**.

Cream coloured solid, yield: 6.4 gm (85%), mp: 126-128 °C; IR (KBr): 3201 (NH), 1695 (ester-C=O), 1676 (piperidine-C=O), 1655 (amide-C=O); ^1H NMR (400 MHz, $CDCl_3$): δ 1.26-1.30 (t, J = 7.08 Hz, 3H, $CH_2C\underline{H}_3$), 1.37-1.40 (t, J = 7.18 Hz, 3H, $CH_2C\underline{H}_3$), 2.89-2.92 (m, 2H, CH_2, piperidine), 3.68-3.71 (m, 2H, CH_2, piperidine), 4.15-4.20 (q, J = 7.12 Hz, 2H, $C\underline{H}_2CH_3$), 4.26 (s, 2H, CH_2-acetamido), 4.34-4.39 (q, J = 7.11 Hz, 2H, $C\underline{H}_2CH_3$), 4.56 (s, 2H, CH_2, piperidine), 12.10 (br s, 1H, NH) ppm; ^{13}C NMR (100 MHz, $CDCl_3$, CPD): δ 14.51, 14.88, 41.26, 42.35, 42.78, 61.22, 61.86, 112.79, 146.99, 155.67, 163.83, 165.86 ppm.

2.8.4. Synthesis of diethyl 2-(2-(4-methylpiperazin-1-yl)acetamido)-4,7-dihydrothieno[2,3-c] pyridine-3,6(5H)-dicarboxylate (5)

To a suspension of the intermediate **4** (0.001 mol; 0.375 gm) in 3 ml of dry tetrahydrofuran (THF) added 1-methylpiperazine (0.0015 mol) dropwise and stirred at 60 °C for two hours. After completion of the reaction (as monitored by TLC), the excess THF was evaporated under reduced pressure, the resulting residue was triturated with water and filtered to obtain crude product. Recrystallization of crude compound with absolute alcohol resulted in pure final compound **5** (**Maybridgehit MB-41570**).

Golden-yellow solid, yield: 350 mg (80%), mp: 95-97 °C; IR (KBr): 3229 (NH), 1659 (ester-C=O), 1562 (piperidine-C=O), 1516 (amide-C=O); ^{1}H NMR (400 MHz, $CDCl_3$): δ 1.26-1.29 (t, *J* = 7.01 Hz, 3H, $CH_2C\underline{H}_3$), 1.36-1.40 (t, *J* = 7.20 Hz, 3H, $CH_2C\underline{H}_3$), 2.45 (s, 3H, N-$C\underline{H}_3$), 2.75 (s, 8H, 4CH_2-piperazine), 2.89 (s, 2H, CH_2, piperidine), 3.28 (s, 2H, CH_2-acetamido), 3.68-3.69 (m, 2H, CH_2, piperidine), 4.14-4.19 (q, *J* = 7.06 Hz, 2H, $C\underline{H}_2CH_3$), 4.33-4.38 (q, *J* = 7.06 Hz, 2H, $C\underline{H}_2CH_3$), 4.55 (s, 2H, CH_2, piperidine), 12.24 (br s, 1H, NH) ppm; ^{13}C NMR (100 MHz, $CDCl_3$, CPD): δ 14.34, 14.67, 41.64, 45.45, 52.68, 54.61, 60.50, 60.74, 61.61, 147.34, 155.50, 165.34, 168.14 ppm.

2.8.5. Procurement and characterization of ChemBridgehit (CB-10358).

The ChemBridgehit "CB-10358" was procured directly from the drug database provider (ChemBridge Corporation, San Diego, USA) and confirmed its structure based on ^{1}H and ^{13}C NMR.

^{1}H NMR (400 MHz, $CDCl_3$): δ 1.23-1.29 (t, *J* = 7.01 Hz, 3H, $CH_2C\underline{H}_3$), 2.17-2.45 (m, 6H, piperidine), 2.79 (m, 1H, piperidine), 2.9-3.0 (m, 1H, piperidine), 3.18-3.22 (m, 2H, CH_2), 3.38-3.46 (m, 2H, CH_2, 1H, piperidine), 3.64-3.74 (br s, 6H, OCH_3), 4.15-4.20 (q, *J* = 7.06 Hz, 2H, $C\underline{H}_2CH_3$), 6.20 (s, 1H, Ar-H), 6.93 (s, 2H, Ar-H), 11.46 (br s, 1H, NH) ppm; ^{13}C NMR (100 MHz, $CDCl_3$, CPD): δ 14.07 ($\underline{C}H_3$-CH_2), 25.29 ($\underline{C}H_2$-piperidine), 31.98 ($\underline{C}H_2$-piperidine), 32.09 ($\underline{C}H_2$-CH_2), 34.98 ($\underline{C}$H-piperidine), 50.45 ($\underline{C}H_2$-piperidine), 52.74 ($\underline{C}H_2$-piperidine), 53.04 (O-$\underline{C}H_3$), 53.23 (O-$\underline{C}H_3$), 55.34 (CH_2-$\underline{C}H_2$), 61.31 ($\underline{C}H_2CH_3$), 96.86, 98.15, 98.22 (Ar-C), 139.81 (Ar-$\underline{C}$-N), 167.50 ($\underline{C}$-OCH_3), 167.73 ($\underline{C}$-OCH_3), 171.87 (C=O), 172.92 (C=O) ppm.

2.9. Pharmacological evaluation

2.9.1. Evaluation of hits against the steady-state basal and MT-stimulated KSP ATPase activities

The experiments were performedat 25 °C using a 96-well Sunrise photometer (Tecan, Mannesdorf,Switzerland) at a final volume of 100 μL per well. Steady-state basal and MT-stimulated ATPase rates were measured using the pyruvate kinase/lactate dehydrogenaselinkedassay in buffer A25A [25 mmol/L potassium ACES (pH 6.9),2 mmol/L magnesium acetate, 2 mmol/L potassium EGTA, 0.1 mmol/L potassium EDTA, 1 mmol/L β-mercaptoethanol]. The amounts of KSP were optimized at 80-100 nM for the basal and 5 nM for the MT-stimulated activity assays. The IC_{50} values for the inhibition of the basal and MT-stimulated ATPase activities of Eg5 were measured for K-858 (positive control) between 1 and 200 μM. The ATP concentration was fixed at 1 mM. For the inhibition of the MT-stimulated ATPase activity, the MT concentration was 1μM. The data were analyzed usingKaleidagraph 3.0 (Synergy SoftwareReading, PA) and Microsoft Excel to obtain IC_{50} values (Talapatra et al., 2013; Nagarajan et al., 2012).

3.Results and discussion

3.1. Common feature pharmacophore generation

Ten common feature-based pharmacophore models were generated using a training set of ligands. The scores of the obtained pharmacophore models ranged from 74.029to 68.245and each of the pharmacophore models had a minimum of four features(Table 1). These models vary in their orientation,vector directions, and composition. Essentially, the major structural requisite determined by DS consists of ring aromatic (R), hydrogen bond acceptor (A), positively ionizable (P) or hydrophobic (H) feature for favourable interactions. The Direct Hitbit mask is the ligand that directly match the pharmacophore and the value '1' indicates that the molecule maps to every feature in the pharmacophore. The Partial Hit bit mask is the ligand that partially match the pharmacophore and the value '0' indicates the complete matching with the pharmacophore. The positively ionizable (P) pharmacophoric feature and hydrogen bond acceptor (A) were observed as common features among all the ten pharmacophore models. This is in agreement with the presence of basic amino groups and hydrogen bond acceptor atoms in structural features of all the training set molecules. The top-ranked pharmacophore model (Hypo1) was chosen as the best model based on scores, fit values, the presence of the number of pharmacophoric features and feature diversity (Tables 1 and 2). The proposed modes of pharmacophore mapping of the training set ligands on this model were found to be good and in accordance with fit values. The best model (Hypo1) contains one ring aromatic (R), one positively ionizable (P), one hydrophobic (H), and two hydrogen bond acceptors (A_1 and A_2) features. Hypo1 was found to becompetentadequately to map the training set molecules and canbe applied effectively to recognize the potential KSP inhibitory ligands from drug databases.The distance between two hydrogen bond acceptors (A_1 and A_2) was determined as 3.510 Å. The hydrogen bond acceptor 1 (A_1) was located at a distance of 4.654 Å from the hydrophobic feature (H) and the feature P (6.080 Å), respectively. The hydrogen bond acceptor 2 (A_2) was distanced from the ring aromatic (R) feature at 3.653 Å and hydrophobic (H) feature at 5.048 Å. Three features (P, R, and H) are positioned in atriangular fashionwherein the distance between ‘P’ and ‘R’ was found to be 7.947 Å, while the distance between ‘P’ and ‘H’ features was determined to be 8.364 Å (Figure 7A).The highly active molecule of the training set (**2**) mapped all the pharmacophoricfeatures effectively on Hypo1 (Figure 7B).

3.2. Validation

The pharmacophore models were validated using a test set comprising of active and inactive KSP inhibitors (Table 3 and Supplementary Table S1). The test set constitutes a total of 809 ligands (active: 54andinactive: 755). The top-ranked pharmacophore model (Hypo1) was validatedcorrespondingly using a test set by defining Maximum Omitted Feature value as ‘0’. Hypo1 screened 48 compounds (highly active=34 and moderately active=14) as active out of 54 known active ligands (88.88%) and 13 compounds as inactive out of 755 known inactive ligands (1.72%) from the test set (Table 3). Hypo1was observed toidentify the active molecules and to distinguish the active from inactive molecules effectively. Finally, Hypo1 was selected as the best pharmacophore model of KSP inhibitors.

3.3.Database screening/searching

The validated pharmacophore model (Hypo1) was subjected to searching in two different databases[Maybridge(MB) and ChemBridge(CB)]constituting 52610 and 74917 ligands, respectively. During the database searching,MaxOmit Feature ‘0’ and fit value > 3 were applied so that molecules that match all the features would be screened. This screening process identified 389 and 632ligands from MB and CB,respectively (Figure 8). Further, molecules were filtered through (i) Lipinski’srule offive and (ii)Veberrule. The implementation of drug-likeliness filter reduced the hits of drug unlikeliness profiles and retrieved 340 and 603 hits from MBand CB databases as drug-like molecules. Further, these hit molecules were filtered to retain the hits with efficient ADMET profiles. The approach filtered 43 and 217 (Total: 260) ligands respectively as hits of necessary pharmacophoric, drug-likeliness, and ADMET profiles. These hits were subjected to molecular docking studies(Figure 8).

3.4. Molecular docking

Molecular docking was employed as a structure-based filter to assess the potential ligands interacting with binding-site residues as well as to predict the probable binding mode of ligands withinthe protein structure. All the hits retrieved from the two different databaseswere subjected to molecular docking to analyzethe capability of binding ofligands inside the binding pocket of KSP.For each of the input ligands, CDOCKER generated numerousreasonable binding conformations and rankedthese on the basis of CDOCKERenergy values. Thus, the ligand-bound conformationbearing the most favourable energy was considered as the best orientation.

Before performing the molecular docking for all the hit molecules, SB-743921 (bound ligand of KSP) and training set (includes SB-743921) ligands were also docked into the crystal structure of KSP (PDB ID: 4BXN) as a part of the validation of the molecular docking protocol.Molecular docking reproduced almost the same binding mode of SB-743921 inside the defined binding pocket with a docking energy of -26.05 kcal/mol(Table 2). The docking pose of SB-743921 (pink coloured ball and stick model) showed favourable interactions with crucial residues within the binding-site of KSP as observed in the crystal structure(yellow coloured ball and stick model) pose (Figure 9). The chromen-4-one moiety of SB-743921 was surrounded by the crucial residues of Trp127, Try211, Glu215, and Ala218, whereas the chloro substituent demonstrated hydrophobic interactions with Leu214 and Lys216, respectively. Similarly, the methyl group on the aromatic ring exhibited hydrophobic interactions with the residues of Leu132 and Ala133 (Figure 9). In 2007, Roeckerand co-workers crystallized KSP with an inhibitor MKR (PDB: 2Q2Y) and revealed a weak hydrogen bond between the carbonyl oxygen of MKR with the hydroxyl group of an aromatic amino acid Tyr211 (3.26 Å)(Roecker et al., 2007).In 2010, Kaan and co-workers reported the phenolic hydroxyl group of (*S*)-enastron interacting with Glu118 of KSP through a hydrogen bond (2.69 Å). Further, a phenyl substituent of the same ligand interacted with aromatic residues (Trp127 and Tyr211) through a π-π stacking interaction and an acidic residue Glu116 exhibited vdW interactions thereby contributing to the higher ligand binding affinity (PDB ID:2X7C)(Kaan, Ulaganathan, Rath, et al., 2010).The same research group crystallized another KSP-inhibitor complex (PDB ID: 2WOG) and identified the existence of a hydrophobic interaction of STLC with the side chain of Glu116(Kaan, Ulaganathan, Hackney, et al., 2010).Recently (2013), the authors deposited the structure of the KSP-ispinesib complex (PDB ID: 4A5Y) in which a strong hydrogen bond prevailed between the free amino group of ispinesib with Glu116 (2.88 Å)(Yi et al., 2013).This has been further evidenced by another KSP structure crystallized with a β-carboline inhibitor (PDB ID:3K3B) which demonstrated the crucial involvement of two different hydrogen bonds for β-carboline NH- and phenolic OH group (substituent) with Glu116 (3.00 Å) and Glu118 (2.66 Å), respectively(Barsanti et al., 2010). The above literature clearly indicated the involvement of the crucial residues Glu116, Glu118, Trp127 and Tyr211 in ligand binding and similar molecular interactions were observed for the docked SB-743921 ligand.

The CDOCKER energies ranged from -26.05 to -33.78 kcal/mol for the training set molecules (which are highly potent) suggesting favourable binding at the KSP binding-site(Table 1). Further, molecular docking was performed for all the hit molecules resulting from database screening. Molecular docking experiments indicated the most favourable binding for the top-rankedhit molecules of Maybridge(MB-41570,CDOCKER energy: -42.70 kcal/mol)and ChemBridge (CB-10358, CDOCKER energy: -39.13 kcal/mol). It was observed that the two hits displayed higher CDOCKER energies indicating the most favourable binding. The KSP docked complexes of MB-41570 (Maybridge)(Figure 10)and CB-10358 (ChemBridge)(Figure 11) were found to have top-ranked CDOCKER energy values. These complexes were then subjected to MD simulations to further substantiate the CDOCKER energies of the hits. The CDOCKER energy values and molecular interactions of bound ligand, training set ligands, and top-ranked hits (Figure 12) from each database are presented in Table S2 of the supplementary material section. The top-ranked complex from each database and the corresponding fit values are also depicted (Supplementary Table S3).

3.5. Binding free energies

The MD studies were conducted for the top-ranked hits retrieved from molecular docking approach (Figure 9) as well as the co-crystallized ligand (SB-743921). After 5ns MD simulation, the binding free energies were computed to identify the inhibitory potential of the two hits and SB-743921. SB-743921 has shown very high *in vitro*potency against KSP (IC_{50}=0.1 nM) and the computed binding free energy of SB-743921 was used as a reference for the assessment of binding affinity of other hit molecules(Talapatra et al., 2013). The calculated binding free energy for SB-743921 at the binding-site of KSP was -31.54 kcal/mol.The binding free energies of hit molecules were found to be -42.89 and -47.53 kcal/molfor MB-41570 (Maybridge) and CB-10358 (ChemBridge)respectively. These two hit molecules therefore show stronger binding free energy values than the reference molecule SB-743921. Further, MB-41570 (Maybridge) and CB-10358 (ChemBridge) were predicted as the most promising candidatesfor KSP inhibition (Table 5). The van der Waals (vdW) and electrostatic energies of MB-41570 and CB-10358 were found to be -52.15±4.54kcal/mol and -51.73±3.53kcal/mol, respectively. The vdWinteractions energy has highly contributed to the ligand binding affinity of the identified hits.In the future, this study may help us to designand develop variousanalogs of MB-41570 and CB-10358asprobable potent KSP inhibitors forcancer chemotherapy.

3.6. Post molecular dynamics analysis

The stability of the protein-ligand complexes (i) 4BXN-SB743921, (ii) 4BXN-MB41570,and (iii) 4BXN-CB10358 was analyzed over 5ns MD simulation by computing RMSD, RMSF, and RoG.The ligand-protein complex of hit molecules showeda marginal variation as compared to reference during the entire simulation suggesting the ligand bound complex of hit molecules as stable as the reference. The RMSD values for the complexes4BXN-SB743921, 4BXN-MB41570,and 4BXN-CB10358 were determined as 2.45, 2.79, and 2.37,respectively(Table 6 and Figure 13).

The flexibility of amino acids for the complexes 4BXN-SB743921, 4BXN-MB41570,and 4BXN-CB10358 was analyzed by assessing the root mean square fluctuations (RMSF) from MD trajectories (Figure 14). The overall RMSF was found to be 0.92, 0.98 and 0.93,respectively for 4BXN-SB743921, 4BXN-MB41570and 4BXN-CB10358 complexes. The complex of 4BXN-MB41570and 4BXN-CB10358 indicatedslightly higher amino acid flexibility than the reference. However, the identical trend in the fluctuation of amino acid residues was observed in all three complexes. The highest magnitude of flexibility was observed around residues10-25, 35-45, and 230-245.

The radius of gyration (RoG) is defined as the moment of inertia of the group of atoms from their centroid of mass. Computation of RoG during the simulation sheds light on the stability of the system.Figure 15presents theRoG over 5ns simulations in the4BXN-SB743921, 4BXN-MB41570and 4BXN-CB10358 complexes. The complex of 4BXN-MB41570has shown highestRoG after the 0.5ns simulation.The simulation beyond 2nsresulted in a decreased RoG. The average RoG for the complexes of 4BXN-SB743921,4BXN-MB41570 and 4BXN-CB10358 was 20.97, 21.03and 20.87, respectively. The results suggestedthat the relatively close stability of the complexes during the MD simulations.

3.7. Synthesis and characterization of Maybridgehit

The Maybridgehit (MB-41570) was synthesized through a convenient synthetic route (Ismail et al., 2012) as shown in scheme-1. Structures of all the synthesized compounds were characterized based on their physicochemical and spectral (IR, ^{1}H NMR and^{13}C NMR) analysis. The spectra of the newly synthesized compounds along with their anticipated structures are presented in the supplementaryinformation. Ethyl 4-oxo-piperidine-1-carboxylate **1** reacted with ethyl cyanoacetate**2** and sulphur in absolute ethanol in the presence of diethylamine afforded the key starting material, diethyl 2-amino-4,7-dihydrothieno[2,3-*c*]- pyridine-3,6(5*H*)-dicarboxylate (**3**) quantitatively. The FT-IR spectrum of **3**, we observed a reasonably sturdy and characteristic bands around 3422, 3318 cm^{-1} accounting for N-H stretching of primary amine. Further, a couple of prominent carbonyl stretching frequencies were observed at 1685 and 1665 cm^{-1} which was attributed to the ester-C=O and piperidine-C=O, respectively. The structure of **3** was elucidated by ^{1}H NMR spectrum (400 MHz), wherein the appearance of an informative broad singlet signal at δ 5.5 ppm attributing to NH$_2$protons. Further, appearance of additional triplet (δ = 1.30-1.35 ppm) and quartet (δ = 4.21-4.27 ppm) signals corresponding to CH_2-$C\underline{H}_3$ and $C\underline{H}_2$-CH_3,respectivelyindicated the formation of the desired starting material **3** via the well-known Gewald reaction. This has been further validated by the appearance of deshielded carbon signals at δ 165.94, 162.51, and 155.71 ppm attributable to $\underline{C}$-NH$_2$, N-$\underline{C}$=O, and C-$\underline{C}$=O respectively in ^{13}C NMR. Moreover, carbon signals in respect to that of ethyl groups appeared at δ 14.58, 14.86, 59.78, and 61.71 ppm in the shielded region confirmed the formation of **3**. Reacting the amino group in **3** with chloroacetyl chloride in the presence of an organic base (triethylamine) resulted an intermediate, diethyl 2-(2-chloroacetamido)-4,7-dihydrothieno[2,3-*c*]pyridine-3,6(5*H*)-dicarboxylate **4**. Thisamide formation was further confirmed by the appearance of NH stretching band at 3201 cm^{-1} anddisappearance of primary amino stretching band in its FT-IR spectrum. Moreover appearance of additional C=O bond stretching at 1655 cm^{-1}has been assigned as carbonyl group of amide. The ^{1}H NMR of **4** showed a broad singlet in the shielded region at δ 12.1 ppm for amide -NH apart from the appearance of acetamido methylene proton at δ 4.26 ppm as a singlet. This has been further evidenced in the ^{13}C NMR where the signal corresponding to acetamido carbonyl was appeared at δ 163.83 ppm apart from the appearance of acetamido methylene signal in the shielded region (δ = 41.26 ppm). Nucleophilic displacement of chlorine in **4** with secondary heterocyclic amine such as *N*-methyl piperazine in tetrahydrofuran yielded the final compound **5**. The ^{1}H NMR of **5** indicated the appearance of additional alicyclic proton in the shielded region as singlet at δ 2.75 ppm corresponding to eight protons of piperazinemoiety, apart from the appearance of one singlet signal at δ 2.45 ppm for N-$C\underline{H}_3$ protons. Similarly, ^{13}C NMR data corroborated well with the appearance of characteristic *N*-methyl carbon at δ 45.45 ppm apart from the carbon signals of piperazine moiety in the upfield region. All the above data confirmed the successful formation of the final compound **5** (Maybridgehit MB-

41570).

3.8. Pharmacological evaluation of hit compounds

3.8.1. Inhibition of hits against the steady-statebasal KSP and MT-stimulated KSP ATPase activities

In silico identified hits (Maybridge: MB-41570and ChemBridge: CB-10358) were evaluated against the basal and MT-stimulated KSP ATPase activities using standard reported protocols(Talapatra et al., 2013; Nagarajan et al., 2012). From the concentration-response curves obtained(seesupplementary information), it was observed that the two identified hitswere unable to displayinhibition against the basal or the MT-stimulated KSP ATPase.

4. Conclusion

In this study, pharmacophore models were developed using ligand-based approachesand validated against a test set of KSP inhibitors. The validated pharmacophore model (Hypo1) exhibited one ring aromatic (R), one positively ionizable (P), one hydrophobic (H), and two hydrogen bond acceptors (A_1 and A_2) asessential features for KSP inhibition. This Hypo1 was used for virtual screening to identify potentKSP inhibitor scaffolds. Subsequently, thesescaffoldswere subjected to moleculardocking and molecular dynamics followed by the calculations of binding free energies. Finally, two ligands (MB-41570 and CB-10358) wereidentified as potentialand easily obtainable or synthesizable(Nankervis et al., 2011; Plater, Murdoch, Morphy, Rankovic, & Rees, 2000)KSP inhibitors. Since the two identified hits (MB41570 and CB10358) demonstrated similar interactions as compared to SB-743921 and exhibited higher binding energies, we synthesized these and evaluated them against the basal and the MT-stimulated KSP ATPase activities. Even though the identified hits had pharmacophoric feature similarities to SB-743921, they displayed no *in vitro* KSP enzyme inhibition.However, the pharmacophore model, interaction analysis, and the systematic protocol of the present study contributes to our understanding of KSP inhibition and may help future medicinal chemists in developing new KSP inhibitors by taking our research findings into account.

Acknowledgments

Authors are thankful to Discipline of Pharmaceutical Sciences, College of Health Sciences, University of KwaZulu-Natal (UKZN), Durban, South Africa for providing the necessary facilities. One of the authors (CB) gratefully acknowledgesNational Research Foundation (DST-NRF), South Africafor research funding in the form of Innovation Post DoctoralResearch Fellowship (ID: 99546).Authors also sincerely thank Centre for High Performance Computing (CHPC), Cape Town, South Africa for computational resources.

Disclosure statement

Authors hereby declare that there are no financial/commercial conflicts of interest.

References

Barsanti, P. A., Wang, W., Ni, Z. J., Duhl, D., Brammeier, N., Martin, E., … Walter, A. O. (2010). The discovery of tetrahydro-β-carbolines as inhibitors of the kinesin Eg5. *Bioorganic and Medicinal Chemistry Letters*, *20*, 157–160.https://doi.org/10.1016/j.bmcl.2009.11.012

Berendsen, H. J. C., Postma, J. P. M., van Gunsteren, W. F., DiNola, a, & Haak, J. R. (1984). Molecular dynamics with coupling to an external bath. *The Journal of Chemical Physics*, *81*, 3684–3690. https://doi.org/10.1063/1.448118

Blangy, A., Arnaud, L., & Nigg, E. A. (1997). Phosphorylation by p34(cdc2) protein kinase regulates binding of the kinesin-related motor HsEg5 to the dynactin subunitp150(Glued). *Journal of Biological Chemistry*, *272*, 19418–19424. https://doi.org/10.1074/jbc.272.31.19418

Carbajales, C., Prado, M. Á., Gutiérrez-de-Terán, H., Cores, Á., Azuaje, J., Novio, S., … Coelho, A. (2014). Structure-based design of new KSP-Eg5 inhibitors assisted by a targeted multicomponent reaction. *ChemBioChem*, *15*, 1471–1480. https://doi.org/10.1002/cbic.201402089

Case, D. A., Babin, V., Berryman, J. T., Betz, R. M., Cai, Q., Cerutti, D. S., … Kollman, P. A. (2014). *AMBER 14,* University of California, San Francisco. Retrieved from http:// ambermd.org/

Civelekoglu-Scholey, G., & Scholey, J. M. (2010). Mitotic force generators and chromosome segregation. *Cellular and Molecular Life Sciences*, *67*, 2231–2250. https://doi.org/10.1007/s00018-010-0326-6

Compton, D. A. (2000). Spindle assembly in animal cells. *Annual Review of Biochemistry*, *69*, 95–114. https://doi.org/10.1146/annurev.biochem.69.1.95

Cox, C. D., Coleman, P. J., Breslin, M. J., Whitman, D. B., Garbaccio, R. M., Fraley, M. E., … Hartman, G. D. (2008). Kinesin spindle protein (KSP) inhibitors. 9. Discovery of (2*S*)-4-(2,5-Difluorophenyl)-*N*-[(3*R*,4*S*)-3-fluoro-1-methylpiperidin-4-yl]-2-hydroxymethyl)-*N*-methyl-2-phenyl-2,5-dihydro-1*H*-pyrrole-1-carboxamide (MK-0731) for the treatment of taxane-refractory cancer. *Journal of Medicinal Chemistry*, *51*, 4239–4252. https://doi.org/10.1021/jm800386y

DassaultSystèmes BIOVIA, Discovery Studio Modeling Environment, Release 4.5, San Diego: DassaultSystèmes, 2015.

DeBonis, S., Simorre, J.-P., Crevel, I., Lebeau, L., Skoufias, D. A., Blangy, A., … Kozielski,F. (2003). Interaction of the mitotic inhibitor monastrol with human kinesin Eg5. *Biochemistry*, *42*, 338–349. https://doi.org/10.1021/bi026716j

Duan, L., Liu, X., & Zhang, J. Z. H. (2016). Interaction entropy: A new paradigm for highly efficient and reliable computation of protein-ligand binding free energy. *Journal of the American Chemical Society*, *138*, 5722–5728. https://doi.org/10.1021/jacs.6b02682

El-Nassan, H. B. (2013). Advances in the discovery of kinesin spindle protein (Eg5) inhibitors as antitumor agents. *European Journal of Medicinal Chemistry*, *62*, 614–631. https://doi.org/10.1016/j.ejmech.2013.01.031

Fraley, M. E., Garbaccio, R. M., Arrington, K. L., Hoffman, W. F., Tasber, E. S., Coleman, P. J., … Hartman, G. D. (2006). Kinesin spindle protein (KSP) inhibitors. Part 2: The design, synthesis, and characterization of 2,4-diaryl-2,5-dihydropyrrole inhibitors of the mitotic kinesin KSP. *Bioorganic & Medicinal Chemistry Letters16*, 1775-1779. https://doi.org/10.1016/j.bmcl.2006.01.030

Gerecitano, J. F., O'Connor, O., Van Deventer, H., Hainsworth, J., Leonard, J., Afanasayev, B., … Conlan, M. (2009). A phase I/II trial of the kinesin spindle protein (KSP) inhibitor SB-743921 dosed q14d without and with prophylactic G-CSF in non-Hodgkin lymphoma (NHL) or Hodgkin lymphoma (HL). *Journal of Clinical Oncology*, *27*, (No. 15_suppl, abstr) 8578. https://doi.org/10.1200/jco.2009.27.15_suppl.8578.

Goodson, H. V, Kang, S. J., & Endow, S. a. (1994). Molecular phylogeny of the kinesin family of microtubule motor proteins. *Journal of Cell Science*, *107*, 1875–1884. Retrieved from http://jcs.biologists.org/content/107/7/1875.abstract

Gu, W.-G., Zhang, X., & Yuan, J.-F. (2014). Anti-HIV drug development through computational methods. *The AAPS Journal*, *16*, 674–80. https://doi.org/10.1208/s12248-014-9604-9

Hartman, G. D., Egbertson, M. S., Halczenko, W., Laswell, W. L., Duggan, M. E., Smith, R.

L., … Lynch, R. J. (1992). Non-peptide fibrinogen receptor antagonists. 1. Discovery and design of exosite inhibitors. *Journal of Medicinal Chemistry*, *35*, 4640–4642. https://doi.org/10.1021/jm00102a020

Hirokawa, N. (1998). Superfamily and Dynein Kinesin of and the Mechanism Proteins Organelle Transport. *Science*, *279*, 519–526. https://doi.org/10.1126/science.279.5350.519

Holen, K. D., Belani, C. P., Wilding, G., Ramalingam, S., Volkman, J. L., Ramanathan, R. K., … Ho, P. T. C. (2011). A first in human study of SB-743921, a kinesin spindle protein inhibitor, to determine pharmacokinetics, biologic effects and establish a recommended phase II dose. *Cancer Chemotherapy and Pharmacology*, *67*, 447–454. https://doi.org/10.1007/s00280-010-1346-5

Hou, T., Wang, J., Li, Y., & Wang, W. (2011). Assessing the performance of the molecular mechanics/Poisson Boltzmann surface area and molecular mechanics/generalized Born surface area methods. II. The accuracy of ranking poses generated from docking. *Journal of Computational Chemistry*, *32*, 866–877. https://doi.org/10.1002/jcc.21666

http://www.rcsb.org/pdb/results/results.do?qrid=CA488289&tabtoshow=Current.(n.d.).Retrieved fromhttp://www.rcsb.org/pdb/results/results.do?qrid=CA488289&tabtoshow=Current

https://clinicaltrials.gov (accessed on 09/09/2016).

Ismail, M. M., Kamel, M. M., Mohamed, L. W., Faggal, S. I. & Galal, M. A. (2012). Synthesis and biological evaluation of thiophene derivatives as acetylcholinesterase inhibitors. *Molecules17*, 7217-7231. https://doi:10.3390/molecules17067217

Jiang, C., Chen, Y., Wang, X., & You, Q. (2007). Docking studies on kinesin spindle protein inhibitors: an important cooperative `minor binding pocket' which increases the binding affinity significantly. *Journal of Molecular Modeling*, *13*, 987–992. https://doi.org/10.1007/s00894-007-0219-2

Jorgensen, W. L., Chandrasekhar, J., Madura, J. D., Impey, R. W., & Klein, M. L. (1983). Comparison of simple potential functions for simulating liquid water. *The Journal of Chemical Physics*, *79*, 926. https://doi.org/10.1063/1.445869

Kaan, H. Y. K., Ulaganathan, V., Hackney, D. D., & Kozielski, F. (2010). An allosteric transition trapped in an intermediate state of a new kinesin-inhibitor complex. *The Biochemical Journal*, *425*, 55–60. https://doi.org/10.1042/BJ20091207

Kaan, H. Y. K., Ulaganathan, V., Rath, O., Prokopcovà, H., Dallinger, D., Kappe, C. O., & Kozielski, F. (2010). Structural basis for inhibition of Eg5 by dihydropyrimidines:

Stereoselectivity of antimitotic inhibitors enastron, dimethylenastron and fluorastrol. *Journal of Medicinal Chemistry*, *53*, 5676–5683. https://doi.org/10.1021/jm100421n

Karunagaran, S., Subhashchandrabose, S., Lee, K. W., & Meganathan, C. (2016). Investigation on the isoform selectivity of novel kinesin-like protein 1 (KIF11) inhibitor using chemical feature based pharmacophore, molecular docking, and quantum mechanical studies. *Computational Biology and Chemistry*, *61*, 47–61. https://doi.org/10.1016/j.compbiolchem.2016.01.002

Kholmurodov, K., Smith, W., Yasuoka, K., Darden, T., & Ebisuzaki, T. (2000). A smooth-particle mesh Ewald method for DL_POLY molecular dynamics simulation package on the Fujitsu VPP700. *Journal of Computational Chemistry*, *21*, 1187–1191. https://doi.org/10.1002/1096-987X(200010)21:13<1187::AID-JCC7>3.0.CO;2-7

Liu, F., You, Q.-D., & Chen, Y.-D. (2007). Pharmacophore identification of KSP inhibitors. *Bioorganic & Medicinal Chemistry Letters*, *17*, 722–726. https://doi.org/http://dx.doi.org/10.1016/j.bmcl.2006.10.083

Lyne, P. D., Lamb, M. L., & Saeh, J. C. (2006). Accurate prediction of the relative potencies of members of a series of kinase inhibitors using molecular docking and MM-GBSA scoring. *Journal of Medicinal Chemistry*, *49*, 4805–4808. https://doi.org/10.1021/jm060522a

Michaux, C., de Leval, X., Julémont, F., Dogné, J. M., Pirotte, B., & Durant, F. (2006). Structure-based pharmacophore of COX-2 selective inhibitors and identification of original lead compounds from 3D database searching method. *European Journal of Medicinal Chemistry*, *41*, 1446–1455. https://doi.org/10.1016/j.ejmech.2006.07.017

Nagarajan, S., Skoufias, D. A., Kozielski, F.,& Pae, A. N. (2012). Receptor–ligand interaction-based virtual screening for novel Eg5/kinesin spindle protein inhibitors. *Journal of Medicinal Chemistry*, *55*, 2561–2573. https://doi.org/10.1021/jm201290v

Nankervis, J. L., Feil, S. C., Hancock, N. C., Zheng, Z., Ng, H. L., Morton, C. J., … Parker, M. W. (2011). Thiophene inhibitors of PDE4: Crystal structures show a second binding mode at the catalytic domain of PDE4D2. *Bioorganic and Medicinal Chemistry Letters*, *21*, 7089–7093. https://doi.org/10.1016/j.bmcl.2011.09.109

Neves, M. A. C., Dinis, T. C. P., Colombo, G., & Sá e Melo, M. L. (2009). An efficient steroid pharmacophore-based strategy to identify new aromatase inhibitors. *European Journal of Medicinal Chemistry*, *44*, 4121–4127. https://doi.org/10.1016/j.ejmech.2009.05.003

Pettersen, E. F., Goddard, T. D., Huang, C. C., Couch, G. S., Greenblatt, D. M., Meng, E. C.,

& Ferrin, T. E. (2004). UCSF Chimera-A visualization system for exploratory research and analysis. *Journal of Computational Chemistry*, *25*, 1605–1612. https://doi.org/10.1002/jcc.20084

Plater, M. J., Murdoch, A. M., Morphy, J. R., Rankovic, Z., & Rees, D. C. (2000). Solid phase synthesis of tertiary amines on amide REM resins: Grignard and metal hydride compatible resins. *Journal of Combinatorial Chemistry*, *2*, 508–512. https://doi.org/10.1021/cc000023

Ramesh, M., & Bharatam, P. V. (2014). Importance of hydrophobic parameters in identifying appropriate pose of CYP substrates in cytochromes. *European Journal of Medicinal Chemistry*, *71*,15–23. https://doi.org/10.1016/j.ejmech.2013.10.023

Roe, D. R., & Cheatham, T. E. (2013). PTRAJ and CPPTRAJ: Software for processing and analysis of molecular dynamics trajectory data. *Journal of Chemical Theory and Computation*, *9*, 3084–3095. https://doi.org/10.1021/ct400341p

Roecker, A. J., Coleman, P. J., Mercer, S. P., Schreier, J. D., Buser, C. A., Walsh, E. S., … Hartman, G. D. (2007). Kinesin spindle protein (KSP) inhibitors. Part 8: Design and synthesis of 1,4-diaryl-4,5-dihydropyrazoles as potent inhibitors of the mitotic kinesin KSP. *Bioorganic & Medicinal Chemistry Letters*, *17*, 5677–5682. https://doi.org/10.1016/j.bmcl.2007.07.074

Rosen, L., Chen, L.-C., Iyengar, T., Goldman, J., Lahr, S., Chen, C.-R., … Von Hoff, D. D. (2010). ARQ 621, a novel potent and selective inhibitor of Eg5: Preclinical data and early results from a clinical phase 1 study. *Cancer Research*, *70*, 2750. http://dx.doi.org/10.1158/1538-7445.AM10-2750

Ryckaert, J. P., Ciccotti, G., & Berendsen, H. J. C. (1977). Numerical integration of the cartesian equations of motion of a system with constraints: Molecular dynamics of *n*-alkanes. *Journal of Computational Physics*, *23*, 327–341. https://doi.org/10.1016/0021-9991(77)90098-5

Sakowicz, R., Finer, J. T., Beraud, C., Crompton, A., Lewis, E., Fritsch, A., … Wood, K. W. (2004). Antitumor activity of a kinesin inhibitor. *Cancer Research*, *64*, 3276–3280.

Sarli, V., & Giannis, A. (2008). Targeting the kinesin spindle protein: Basic principles and clinical implications. *Clinical Cancer Research*, *14*, 7583–7587. https://doi.org/10.1158/1078-0432.CCR-08-0120

Saunders, A. M., Powers, J., Strome, S., & Saxton, W. M. (2007). Kinesin-5 acts as a brake in anaphase spindle elongation. *Current Biology*, *17*, R453–R454. https://doi.org/10.1016/j.cub.2007.05.001

Song, H., Zhou, S., Wang, R., & Li, S. (2013). Kinesin spindle protein (KSP) inhibitors in combination with chemotherapeutic agents for cancer therapy. *ChemMedChem*, *8*, 1736–1749. https://doi.org/10.1002/cmdc.201300228

Talapatra, S. K., Anthony, N. G., Mackay, S. P., & Kozielski, F. (2013). Mitotic kinesin Eg5 overcomes inhibition to the phase I/II clinical candidate SB743921 by an allosteric resistance mechanism. *Journal of Medicinal Chemistry*, *56*, 6317–6329. https://doi.org/10.1021/jm4006274

Talele, T. T., Khedkar, S. A., & Rigby, A. C. (2010). Successful applications of computer aided drug discovery: Moving drugs from concept to the clinic. *Current Topics in Medicinal Chemistry*, *10*, 127–141. https://doi.org/10.2174/156802610790232251

Theoclitou, M.-E., Aquila, B., Block, M. H., Brassil, P. J., Castriotta, L., Code, E., … Zheng, X. (2011). Discovery of (+)-*N*-(3-Aminopropyl)-*N*-[1-(5-benzyl-3-methyl-4-oxo-[1,2]thiazolo[5,4-*d*]pyrimidin-6-yl)-2-methylpropyl]-4-methylbenzamide (AZD4877), a kinesin spindle protein inhibitor and potential anticancer agent. *Journal of Medicinal Chemistry*, *54*, 6734–6750. https://doi.org/10.1021/jm200629m

Turner, J., Anderson, R., Guo, J., Beraud, C., Fletterick, R., & Sakowicz, R. (2001). Crystal structure of the mitotic spindle kinesin Eg5 reveals a novel conformation of the neck-linker. *Journal of Biological Chemistry*, *276*, 25496–25502. https://doi.org/10.1074/jbc.M100395200

Veber, D. F., Johnson, S. R., Cheng, H., Smith, B. R., Ward, K. W., & Kopple, K. D. (2002). Molecular properties that influence the oral bioavailability of drug candidates. *Journal of Medicinal Chemistry*, *45*, 2615–2623. https://doi.org/10.1021/jm020017n

Vijayakrishnan, R. (2009). Structure-based drug design and modern medicine. *Journal of Postgraduate Medicine*, *55*, 301–304. https://doi.org/10.4103/0022-3859.58943

Wakui, H., Yamamoto, N., Kitazono, S., Mizugaki, H., Nakamichi, S., Fujiwara, Y., … Tamura, T. (2014). A phase 1 and dose-finding study of LY2523355 (litronesib), an Eg5 inhibitor, in Japanese patients with advanced solid tumors. *Cancer Chemotherapy and Pharmacology*, *74*, 15–23. https://doi.org/10.1007/s00280-014-2467-z

Wang, F., Good, J. A. D., Rath, O., Kaan, H. Y. K., Sutcliffe, O. B., MacKay, S. P., & Kozielski, F. (2012). Triphenylbutanamines: Kinesin spindle protein inhibitors with in vivo antitumor activity. *Journal of Medicinal Chemistry*, *55*, 1511–1525. https://doi.org/10.1021/jm201195m

Woessner, R., Tunquist, B., Lemieux, C., Chlipala, E., Jackinsky, S., Dewolf, W., … Walker, D. (2009). ARRY-520, a novel KSP inhibitor with potent activity in hematological and taxane-resistant tumor models. *Anticancer Research*, *29*, 4373–4380.

Wordeman, L. (2010). How kinesin motor proteins drive mitotic spindle function: Lessons from molecular assays. *Seminars in Cell and Developmental Biology*, *21*, 260–268. https://doi.org/10.1016/j.semcdb.2010.01.018

Wu, G., Robertson, D. H., Brooks, C. L., & Vieth, M. (2003). Detailed analysis of grid-based molecular docking: A case study of CDOCKER - A CHARMm-based MD docking algorithm. *Journal of Computational Chemistry*, *24*, 1549–1562. https://doi.org/10.1002/jcc.10306

Yang, Y. S., Yang, B., Zou, Y., Li, G., & Zhu, H. L. (2016). Design, biological evaluation and 3D QSAR studies of novel dioxin-containing triaryl pyrazoline derivatives as potential B-Raf inhibitors. *Bioorganic and Medicinal Chemistry*, *24*, 3052–3061. https://doi.org/10.1016/j.bmc.2016.05.012

Yi, H., Kaan, K., Major, J., Tkocz, K., Kozielski, F., & Rosenfeld, S. S. (2013). " Snapshots " of ispinesib-induced conformational changes in the mitotic kinesin Eg5. *Journal of Biological Chemistry*, *288*, 18588–18598. https://doi.org/10.1074/jbc.M113.462648

Yin, Y., Sun, H., Xu, J., Xiao, F., Wang, H., Yang, Y., … Wang, L. (2015). Kinesin spindle protein inhibitor SB743921 induces mitotic arrest and apoptosis and overcomes imatinib resistance of chronic myeloid leukemia cells. *Leukemia & Lymphoma*, *56*, 1813–1820. https://doi.org/10.3109/10428194.2014.956319

Yokoyama, H., Sawada, J., Katoh, S., Matsuno, K., Ogo, N., Ishikawa, Y., … Asai, A. (2015). Structural basis of new allosteric inhibition in kinesin spindle protein Eg5. *ACS Chemical Biology*, *10*, 1128–1136. https://doi.org/10.1021/cb500939x

Zhao, H., & Caflisch, A. (2015). Molecular dynamics in drug design. *European Journal of Medicinal Chemistry*, *91*, 4–14. https://doi.org/10.1016/j.ejmech.2014.08.004

Figure Legends

Figure 1.The training set employed for the generation of pharmacophore models.

Figure 2. KSP inhibitors under different stages of clinical development.

Figure3. Pictorial map of KSP representing the three major domains (motor, stalk, and tail).

Figure4. Three-dimensional (3D) arrangement of KSP (ribbon, coloured in grey), inhibitor (SB-743921; magenta sticks) and ADP (shaded in blue) in the crystal structure (PDB ID:

4BXN).

Figure 5. Novel KSP inhibitors designed through molecular modeling approaches.

Figure 6.KSP for molecular docking (**A**) and location of the binding-site sphere (**B**).

Figure 7. (**A**) Best pharmacophore model (Hypo1) and (**B**) Mapping of **2** upon Hypo1.

Figure 8.Flowchart of database screening, drug-like filtrations, molecular docking and molecular dynamics in identifying novel KSP hits.

Figure 9. The orientation of the docked pose (pink coloured ball and stick model) with the cognate ligand (yellow coloured ball and stick model) in the binding-site of KSP.

Figure 10. Interactions of MB-41570 with KSP (Maybridge database).

Figure 11. Interactions of CB-10358 with KSP (ChemBridge database).

Figure 12.Top-ranked hits from each database after molecular docking/MD-MMGBSA.

Figure 13. Root mean square deviation (RMSD) for the complexes of 4BXN-SB743921 (black), 4BXN-MB41570 (red) and 4BXN-CB10358 (green).

Figure 14. Root mean square fluctuations (RMSF) of C-α atoms for 4BXN-SB743921 (black), 4BXN-MB41570 (red) and 4BXN-CB10358 (green) complexes.

Figure 15. Radiation of gyration (RoG) for the complex of 4BXN-SB743921 (black), 4BXN-MB41570 (red) and 4BXN-CB10358 (green).

Scheme 1: Synthetic route for the synthesis of Maybridge hit: Reagents and conditions (a) S, diethylamine, EtOH, 60-70 °C, 2h; (b)$ClCH_2COCl$, *N*,*N*-DMF, rt, 2h; (c) *N*-methyl-piperazine, THF, 50-60 °C, 2 h.

Table Legends

Table 1. Description of common feature pharmacophore models.

Table 2. A training set of molecules for the generation of ligand-based pharmacophore model.

Table 3. Validation of pharmacophore model (Hypo1) using test set.

Table 4.Statistical analysis of top-ranked pharmacophore model (hypo1).

Table 5. MM/GBSA binding free energies of a reference molecule and the best-docked hits in complexation with kinesin spindle protein.

Table 6. Post-dynamics analysis of a reference molecule and the hits in complexation with kinesin spindle protein.

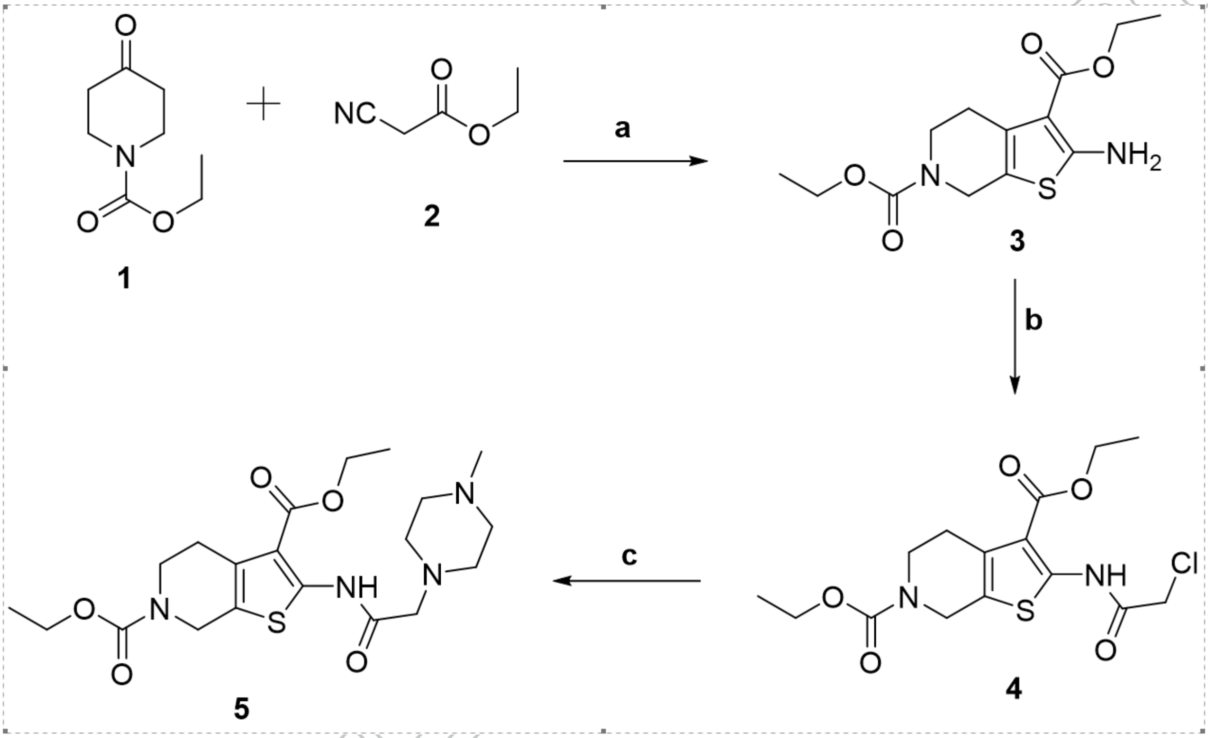
1
2
a
3
b
4
c
5
NC
NH2
NH
Cl
N
O
S

ACCEPTED

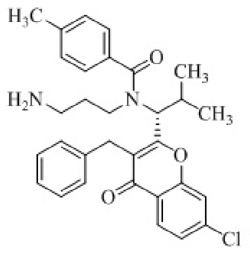

SB-743921 (1)

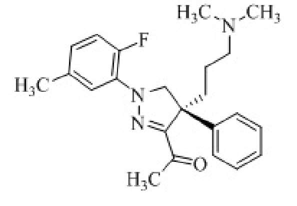

(*R*)-1-(4-(3-(dimethylamino)propyl)-1-(2-fluoro-5-methylphenyl)-4-phenyl-4,5-dihydro-1*H*-pyrazol-3-yl)ethan-1-one **(2)**

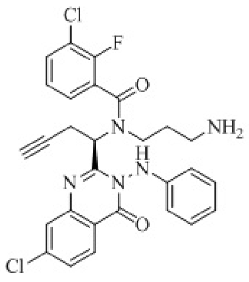

ARQ-621 (3)

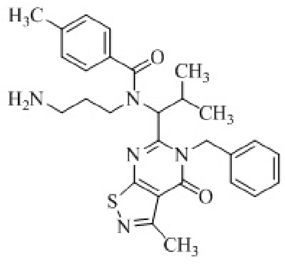

AZD-4877 (4)

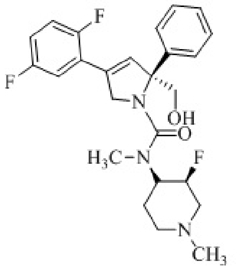

MK-0731 (5)

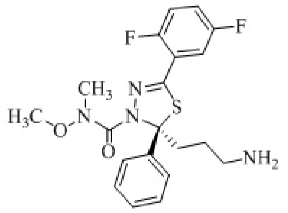

Filanesib (6)

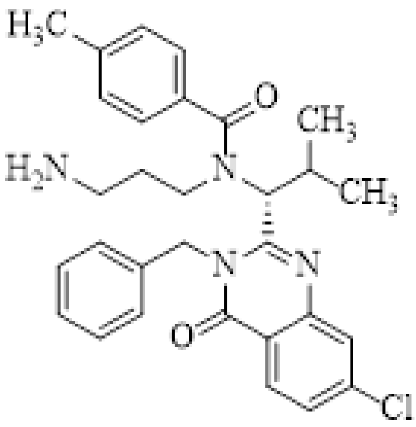

Ispinesib (7)

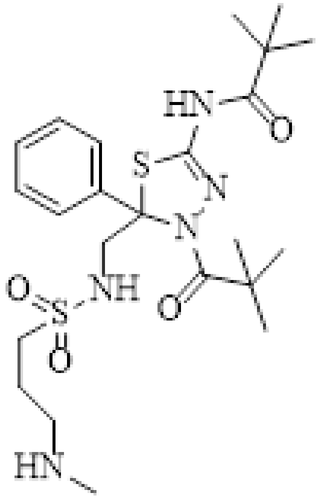

Litronesib (8)

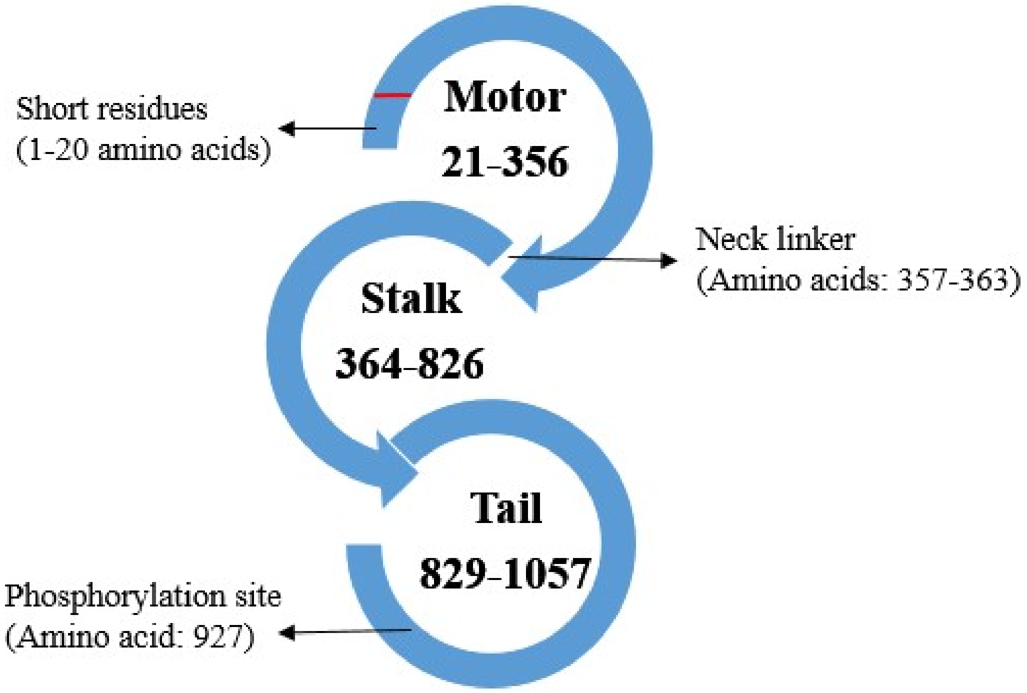
Short residues
(1-20 amino acids)
Motor
21-356
Neck linker
(Amino acids: 357-363)
Stalk
364-826
Tail
829-1057
Phosphorylation site
(Amino acid: 927)

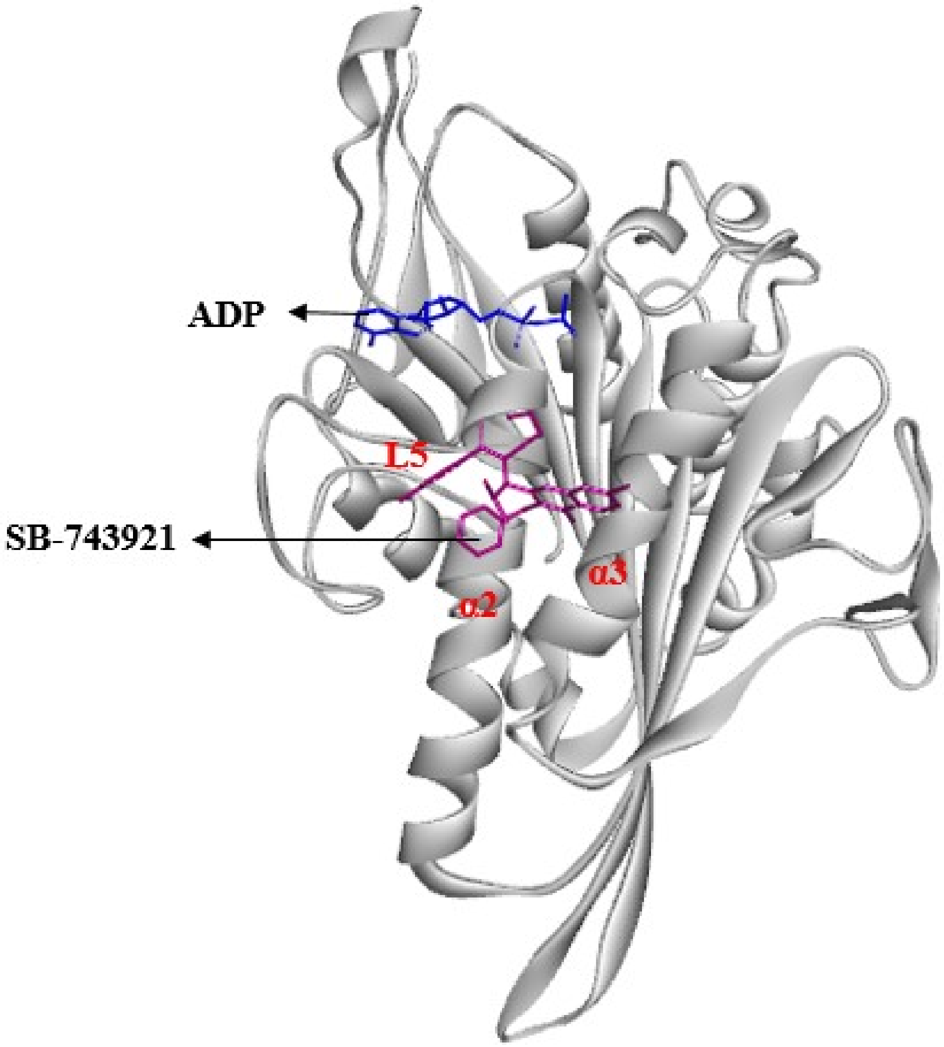
ADP
L5
SB-743921
α3
α2

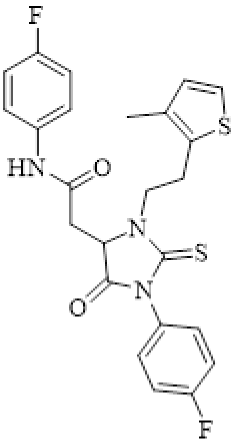

9

IC_{50} = 0.58 μM

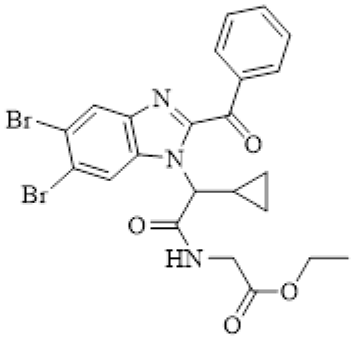

10

IC_{50} = 1.49 μM

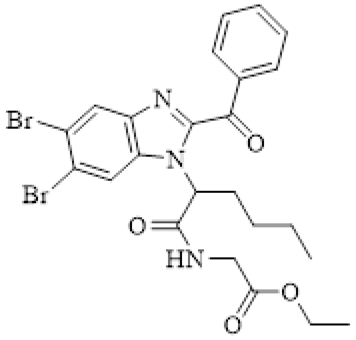

11

IC_{50} = 1.37 μM

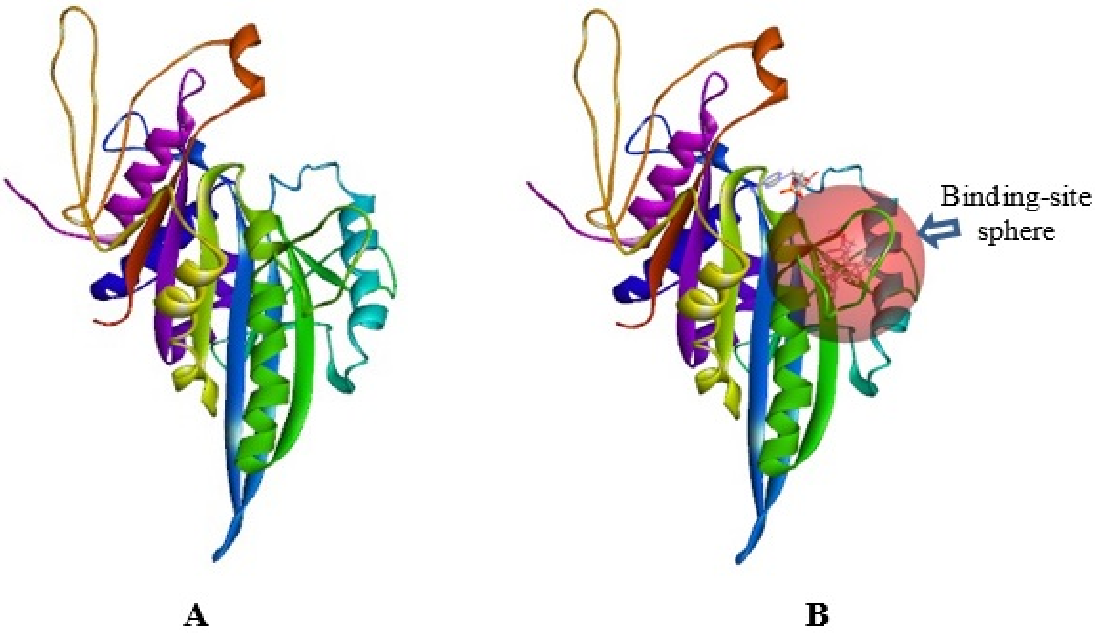
Binding-site sphere
A
B

ACCEPTED MA T

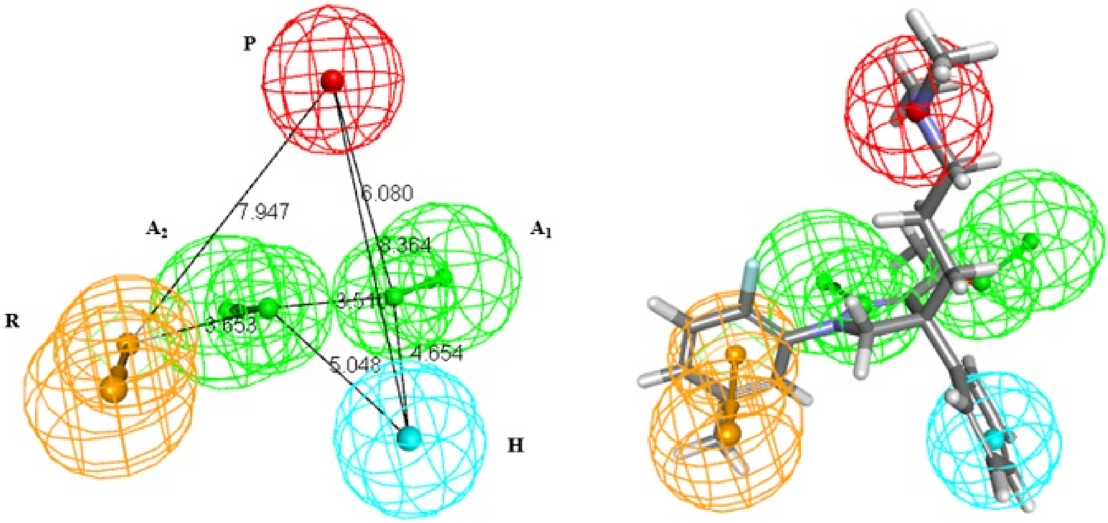
P
7.947
6.080
A2
8.364
A1
R
3.653
5.048
4.654
H

A **B**

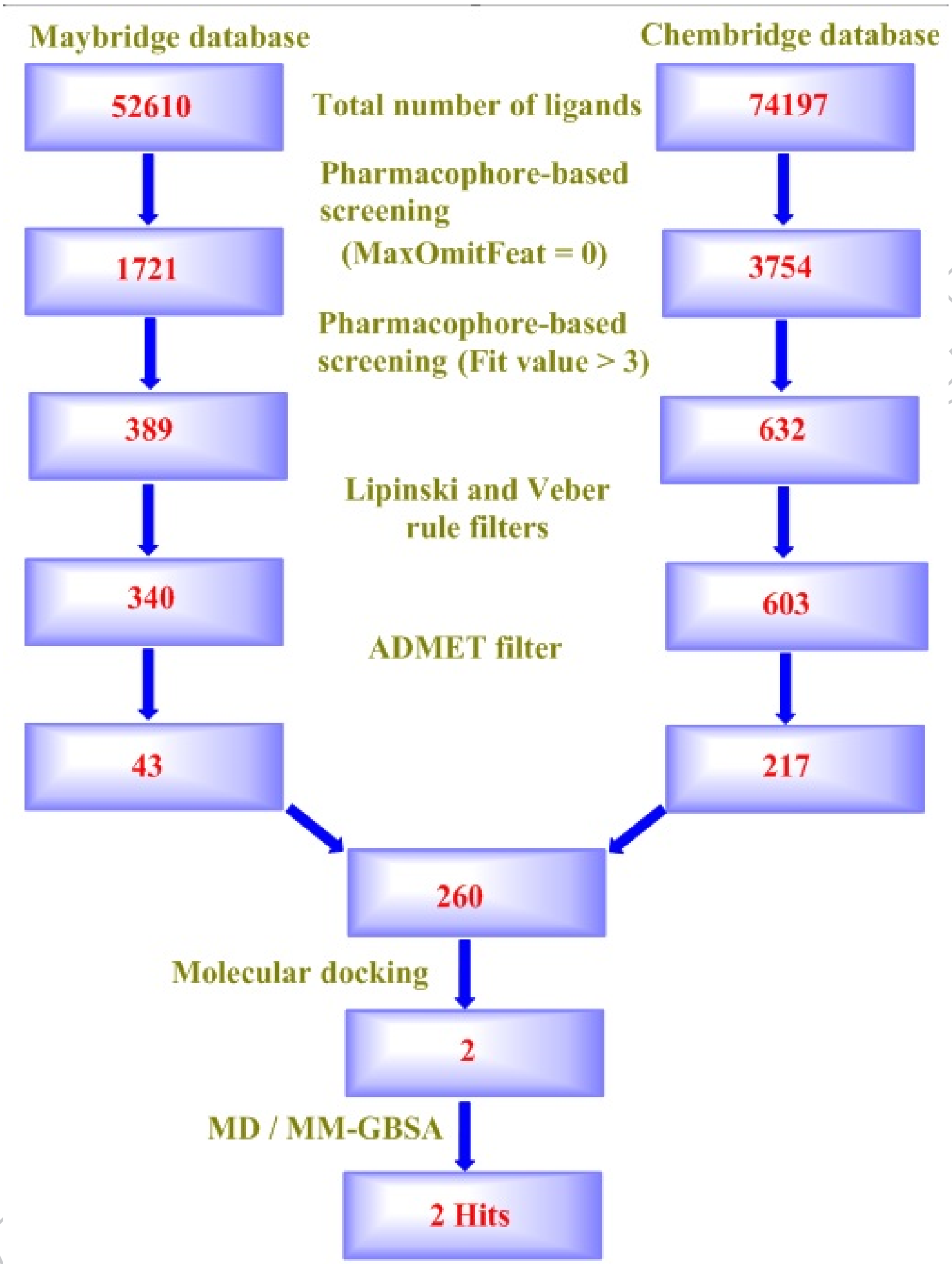
Maybridge database
Chembridge database
52610
Total number of ligands
74197
Pharmacophore-based screening (MaxOmitFeat = 0)
1721
3754
Pharmacophore-based screening (Fit value > 3)
389
632
Lipinski and Veber rule filters
340
603
ADMET filter
43
217
260
Molecular docking
2
MD / MM-GBSA
2 Hits

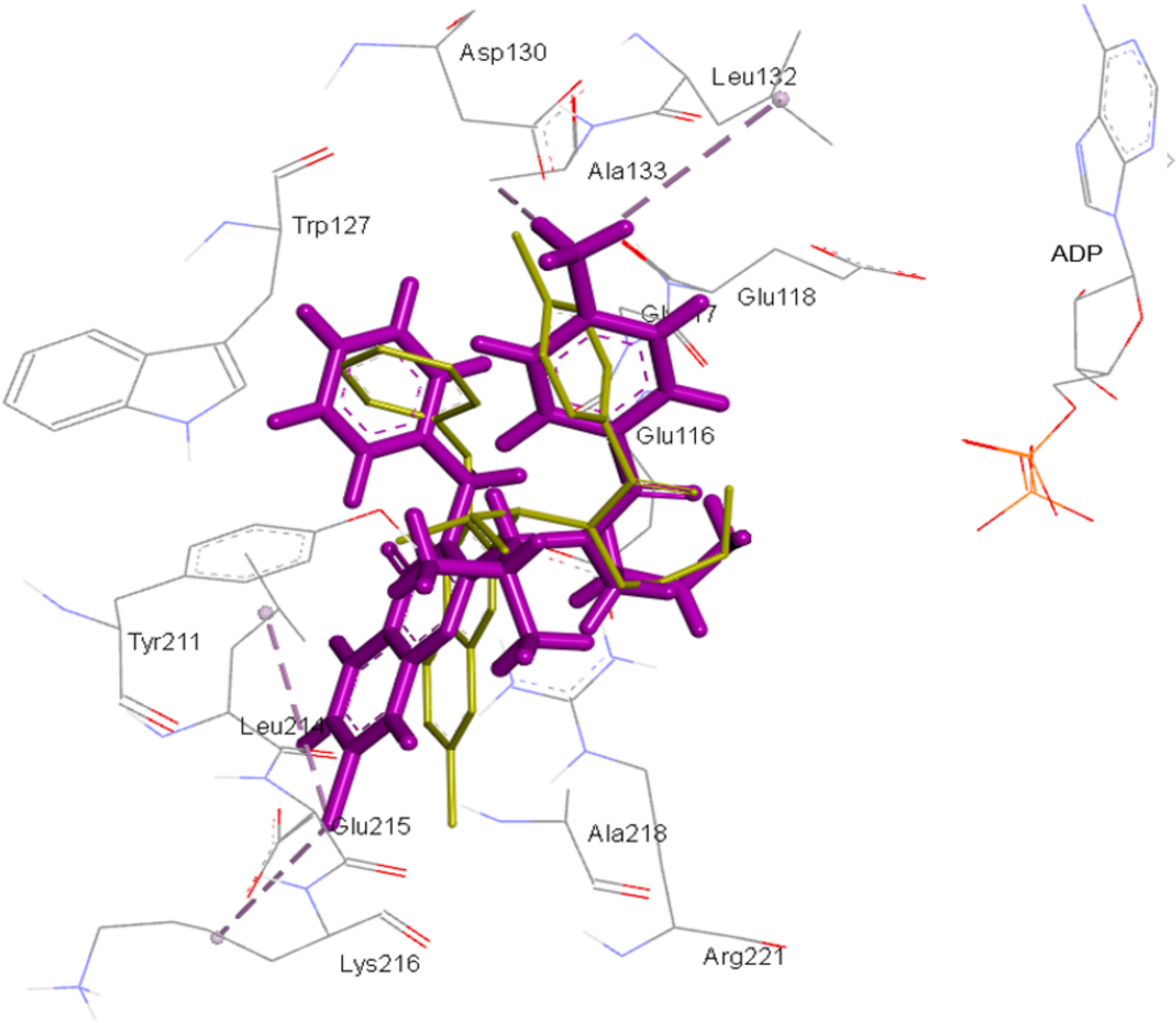
Asp130
Leu132
Ala133
Trp127
ADP
Glu118
Gl 17
Glu116
Tyr211
Leu214
Glu215
Ala218
Lys216
Arg221

ACCE

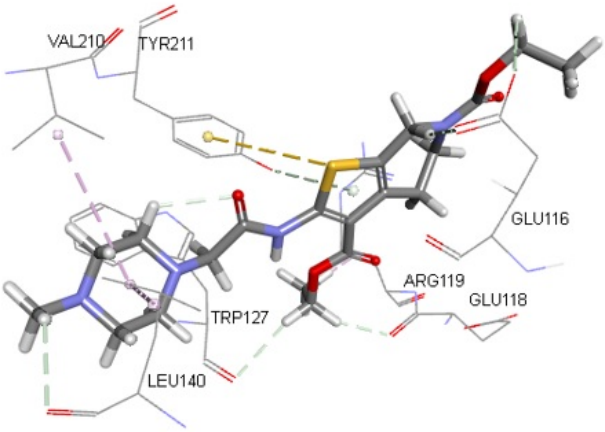
VAL210
TYR211
GLU116
ARG119
GLU118
TRP127
LEU140

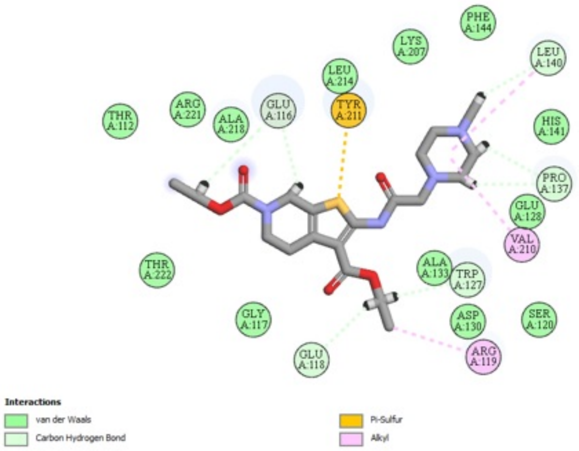
PHE A:144
LYS A:207
LEU A:140
LEU A:214
THR A:112
ARG A:221
ALA A:218
GLU A:116
TYR A:211
HIS A:141
PRO A:137
GLU A:128
VAL A:210
THR A:222
ALA A:133
TRP A:127
GLY A:117
ASP A:130
SER A:120
GLU A:118
ARG A:119
Interactions
van der Waals
Carbon Hydrogen Bond
Pi-Sulfur
Alkyl

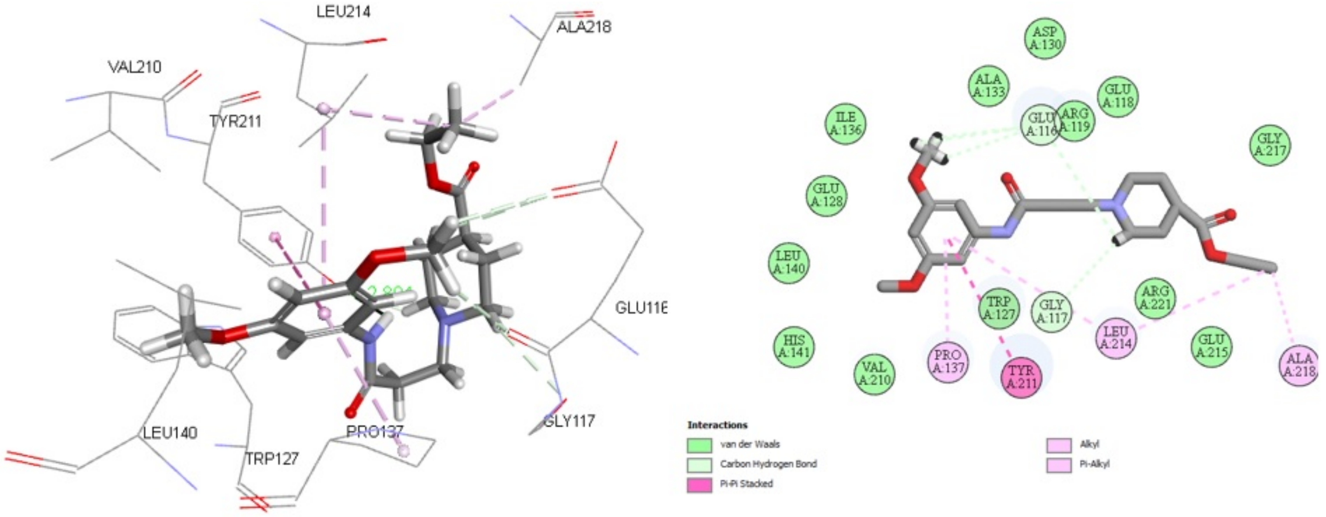
LEU214
ALA218
VAL210
TYR211
GLU118
LEU140
TRP127
PRO137
GLY117
ASP A:130
ALA A:133
GLU A:118
ILE A:136
GLU A:116
ARG A:119
GLY A:217
GLU A:128
LEU A:140
HIS A:141
VAL A:210
PRO A:137
TRP A:127
GLY A:117
TYR A:211
LEU A:214
ARG A:221
GLU A:215
ALA A:218
Interactions
🟩 van der Waals
🟩 Carbon Hydrogen Bond
🟥 Pi-Pi Stacked
🟪 Alkyl
🟪 Pi-Alkyl

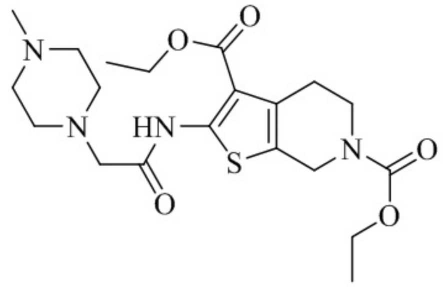

MB-41570 (Maybridge)

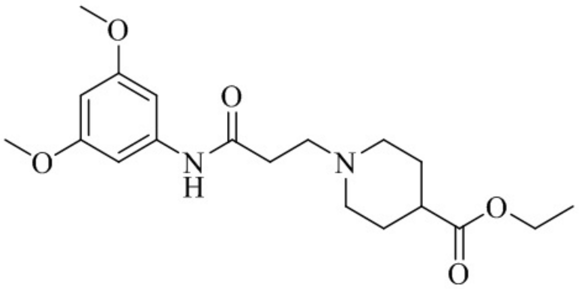

CB-10358 (Chembridge)

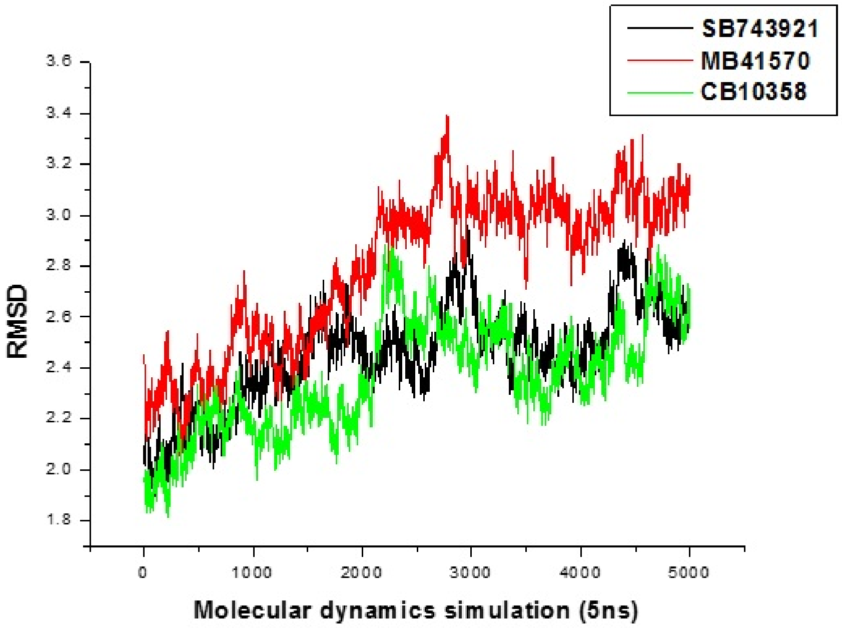
SB743921
MB41570
CB10358
RMSD
3.6
3.4
3.2
3.0
2.8
2.6
2.4
2.2
2.0
1.8
0
1000
2000
3000
4000
5000
Molecular dynamics simulation (5ns)

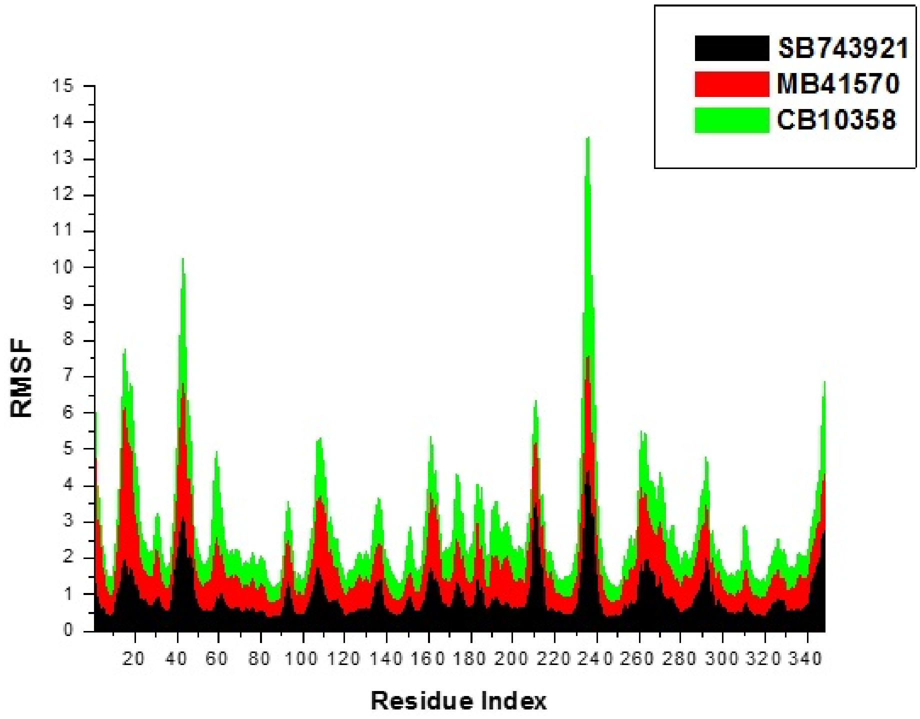
SB743921
MB41570
CB10358
RMSF
0
1
2
3
4
5
6
7
8
9
10
11
12
13
14
15
20
40
60
80
100
120
140
160
180
200
220
240
260
280
300
320
340
Residue Index

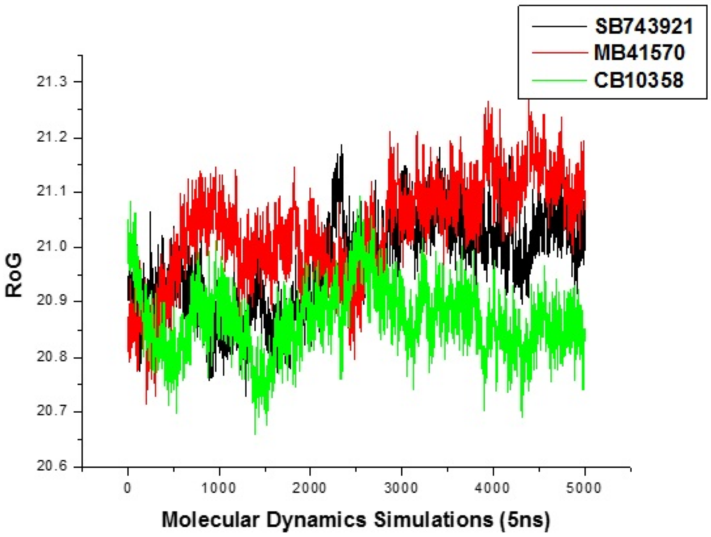
SB743921
MB41570
CB10358
RoG
21.3
21.2
21.1
21.0
20.9
20.8
20.7
20.6
0
1000
2000
3000
4000
5000
Molecular Dynamics Simulations (5ns)

Hypos Rank	**Features**	**Scores**	**Direct Hit**	**Partial Hit**	**Max Fit**
01	RPHAA	74.029	111111	000000	5
02	PHHAA	73.637	111111	000000	5
03	RPHAA	73.610	111111	000000	5
04	PHHAA	69.774	111111	000000	5
05	RRPA	68.876	111111	000000	4
06	RRPA	68.876	111111	000000	4
07	RRPA	68.526	111111	000000	4
08	RRPA	68.276	111111	000000	4
09	RRPA	68.276	111111	000000	4
10	RRPA	68.245	111111	000000	4

No.	Ligands	Features	IUPAC	KSP Inhibition (IC_{50}, nM)	Fit Value	CDOCKER energy
1	SB-743921 (**1**)	RPHAD	(*R*)-*N*-(3-aminopropyl)-*N*-(1-(3-benzyl-7-chloro-4-oxo-4*H*-chromen-2-yl)-methyl-propyl)-4-methyl benzamide	0.1	2.09	-26.05
2	**2**	RPHA	(*R*)-1-(4-(3-(dimethylamino-propyl)-1-(2-fluoro-5-methy-l-phenyl)-4-phenyl-4,5-dihydro-1*H*-pyrazol-3-yl)ethan-1-one	0.2	4.99	-32.63
3	ARQ-621 (**3**)	RPHAD	(*R*)-*N*-(3-aminopropyl)-3-chloro-*N*-(1-(7-chloro-4-oxo-3-(phenylamino)-3,4-dihydro-quinazolin-2-yl)but-3-yn-1-yl)-2-fluoro-benzamide	1.2	1.88	-33.68
4	AZD-4877 (**4**)	RPHA	*N*-(3-aminopropyl)-*N*-(1-(5-benzyl-methyl-4-oxo-4,5-dihydroisothizolo[5,4-*d*]-pyrimidin-6-yl)-2-methyl-propyl)-4-methylbenzamide	2	0.88	-33.47
5	MK-0731 (**5**)	RPHAD	(*S*)-4-(2,5-difluorophenyl)-*N*-((3*S*,4*S*)-3-fluoro-1-methyl-piperidin-4-yl)-2-(hydroxymethyl)-*N*-methyl-2-phenyl-2,5-dihydro-1*H*-pyrrole-1-carboxamide	2.2	0.69	-4.58
6	Filanesib (**6**)	RPHA	(*S*)-2-(3-aminopropyl)-5-(2,5-difluorophenyl)-*N*-methoxy-*N*-methyl-2 phenyl-1,3,4-thiadiazole-3(2*H*)-carboxamide	6	2.44	-33.78

No.	KSP inhibitors	Category of KSP inhibition profile	Biological response (IC_{50})	Total No. of Ligands	Screening by Hypo1
1	Active (Total: 54)	Highly active	< 20 nM	36	34 (94.44%)
		Moderately active	20-100 nM	18	14 (77.77%)
2	Inactive (Total: 755)	Weakly active	> 100 nM	755	13 (1.72%)

Parameters	**Significance**
Total number of molecules in database (D)	809
Total number of active molecules in database (A)	54
Total Hits (Ht)	51
Active Hits (Ha)	48
% Yield of actives [(Ha/Ht) X 100]	94.1
% Ratio of actives [(Ha/A) X100]	88.9
Enrichment factor (E) [(Ha X D)/(Ht X A)]	14.1
False Negatives [A - Ha]	6
False Positives [Ht - Ha]	3
Goodness of Hit Score (GH)[a]	0.9244

[a] [(Ha/4HtA) (3A+Ht)) X (1- ((Ht- Ha)/(D- A))];GH Score 0.9244 indicates good model.

No.	**Molecules**	**Energy components (kcal/mol)**				
		ΔE_{vdW}	**ΔE_{elec}**	**ΔG_{gas}**	**ΔG_{solv}**	**ΔG_{bind}**
1.	SB-743921 (Reference)	-44.40±3.95	-187.56±10.06	-231.96±12.03	200.42±9.10	-31.54±4.33
2.	MB-41570 (Maybridge)	-52.15±4.54	-3.34±4.33	-55.50±7.17	12.60±5.85	-42.89±4.29
3.	CB-10358 (ChemBridge)	-51.73±3.53	-25.77±7.40	-77.50±7.06	77.50±7.06	-47.53±4.09

No.	Molecules	RMSD	RMSF	RoG
1.	SB-743921 (Reference)	2.45	0.92	20.87
2.	MB-41570 (Maybridge)	2.79	0.98	21.03
3.	CB-10358 (ChemBridge)	2.37	0.93	20.87

Ligand and structure based *in silico*studies to identify kinesin spindle protein (KSP) inhibitors as potential anticancer agents

ChandrasekaranBalakumar,[a]MuthusamyRamesh,[a]Chuin Lean Tham,[b]Samukelisiwe Pretty Khathi,[a] Frank Kozielski,[b]CherukupalliSrinivasulu,[a] Girish A. Hampannavar,[a]NisarSayyad,[a] Mahmoud E. Soliman,[a] and RajshekharKarpoormath[a]*

[a]*Discipline of Pharmaceutical Sciences, College of Health Sciences, University of KwaZulu-Natal (UKZN), Westville, Durban 4001, South Africa.*

[b]*Department of Pharmaceutical and Biological Chemistry, The School of Pharmacy, University College London, 29-39 Brunswick Square, London WC1N 1AX, U.K.*

*Corresponding author: karpoormath@ukzn.ac.za (R. Karpoormath)

Supplementary information

Table S1 Test set employed in the validation

S. No	Compd Id	Structure	IC$_{50}$ (nM)	Reference	Category
1	24	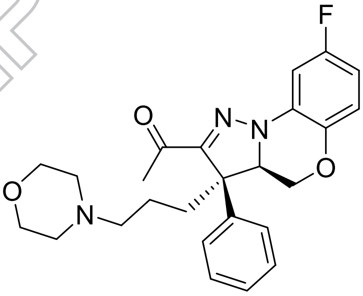	0.4	(Garbaccio et al., 2007)	Active
2	28	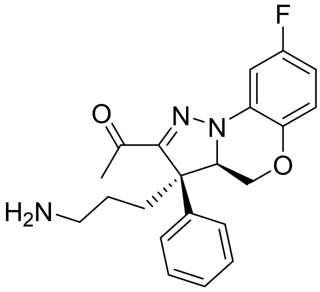	0.5	(Garbaccio et al., 2007)	Active

3	48	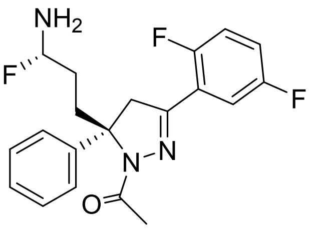	0.82	(Coleman et al., 2007)	Active
4	11	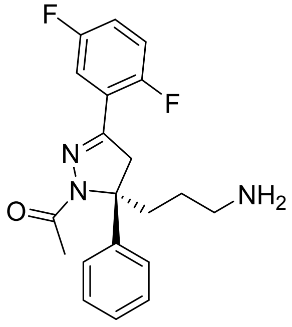	0.9	(Coleman et al., 2007)	Active
5	19	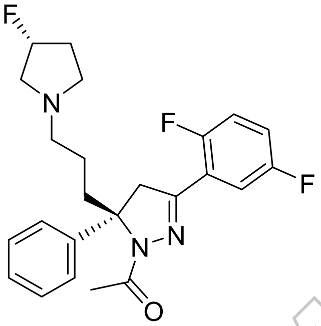	1	(Coleman et al., 2007)	Active
6	26	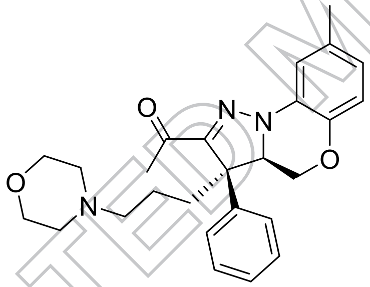	1	(Garbaccio et al., 2007)	Active
7	15	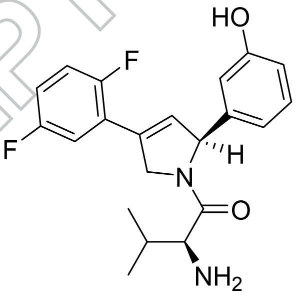	1.2	(Garbaccio et al., 2006)	Active
8	12	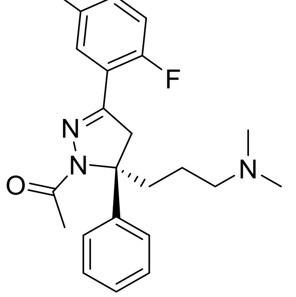	1.4	(Coleman et al., 2007)	Active

9	55	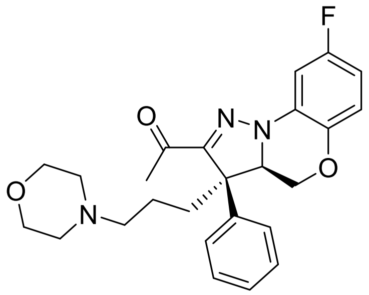	1.6	(Garbaccio et al., 2007)	Active
10	14	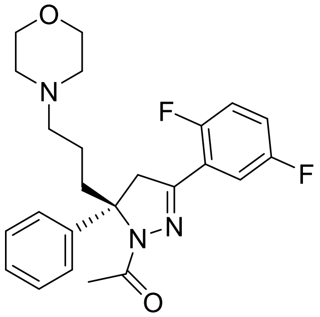	1.8	(Coleman et al., 2007)	Active
11	17	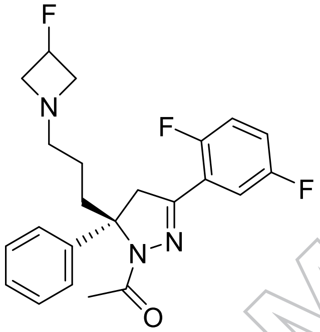	1.8	(Coleman et al., 2007)	Active
12	21	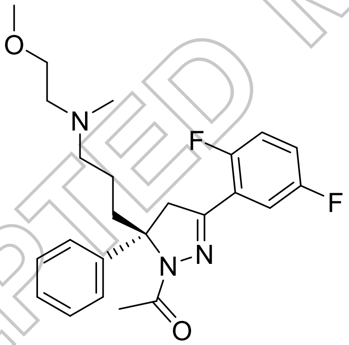	2	(Coleman et al., 2007)	Active
13	62	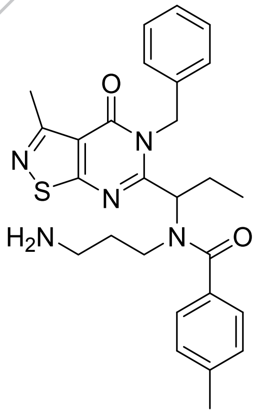	2	(Theoclitou et al., 2011)	Active

14	SCH	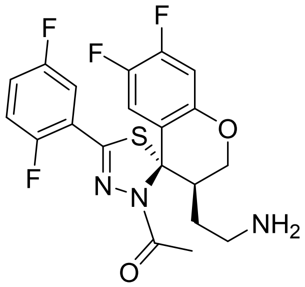	2	(Basso et al., 2010)	Active
15	13	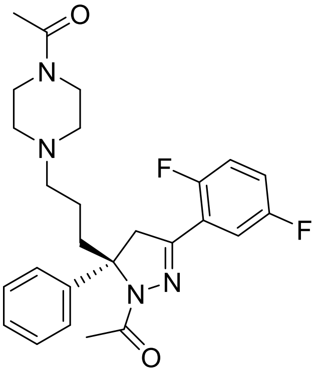	2.8	(Coleman et al., 2007)	Active
16	20	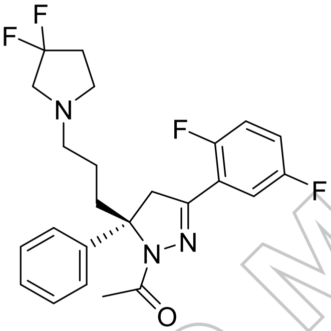	4	(Coleman et al., 2007)	Active
17	29	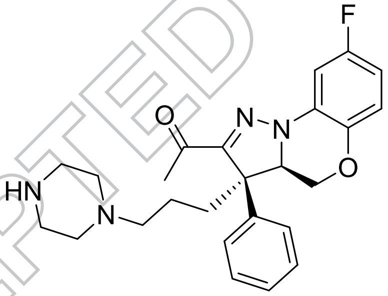	4.3	(Garbaccio et al., 2007)	Active
18	64	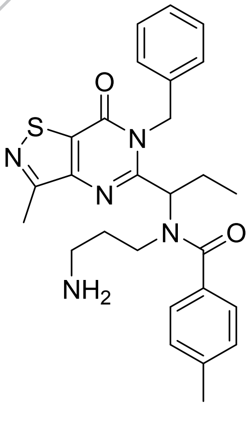	5	(Theoclitou et al., 2011)	Active

19	14	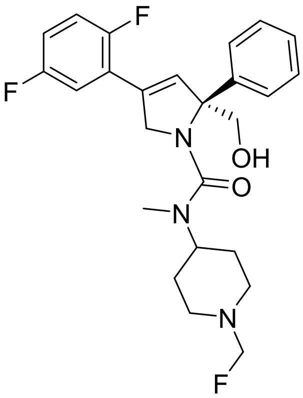	5	(Cox et al., 2008)	Active
20	13	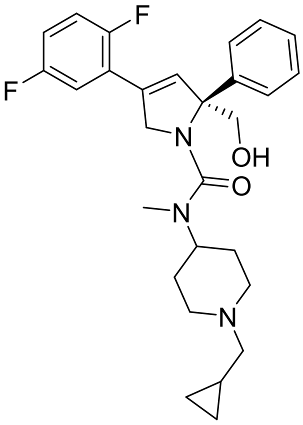	5.1	(Cox et al., 2008)	Active
21	15	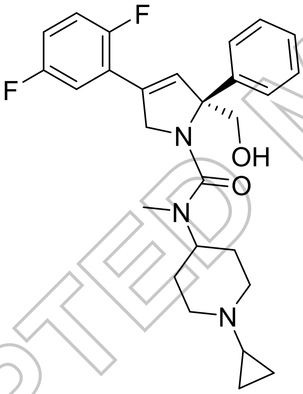	5.9	(Cox et al., 2008)	Active
22	16	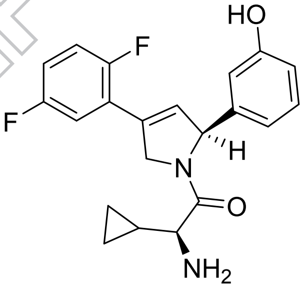	6.5	(Garbaccio et al., 2006)	Active
23	Litronesib	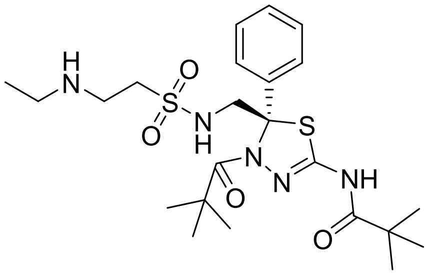	7	(Verschraegen et al., 2014)	Active

24	Pyrrolotriazine	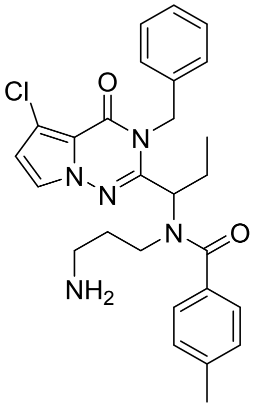	7	(Kim et al., 2006)	Active
25	12	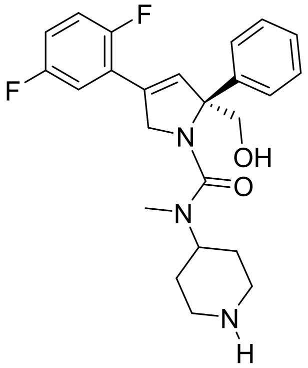	7.4	(Cox et al., 2008)	Active
26	56	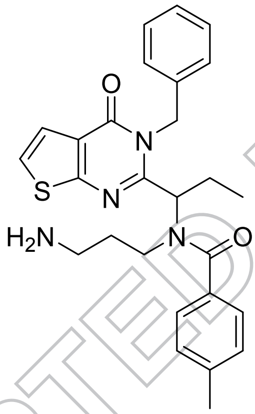	8	(Theoclitou et al., 2011)	Active
27	EMD	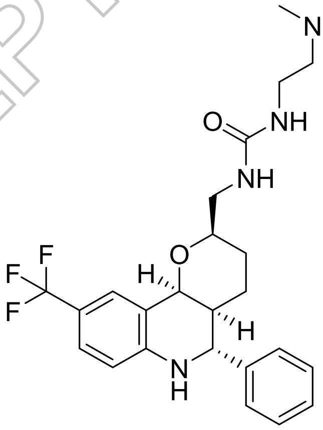	8	(Schiemann et al., 2010)	Active

28	10A	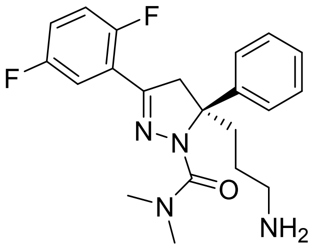	8	(Cox et al., 2006)	Active
29	3	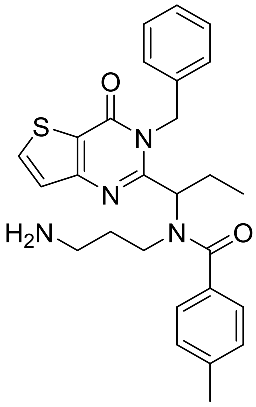	10	(Theoclitou et al., 2011)	Active
30	Ispinesib	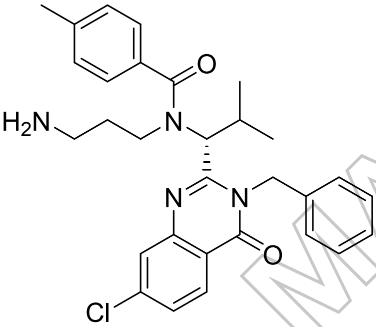	10	(Davis, Sarkar, Hussain, Li, & Sarkar, 2006)	Active
31	Quinazoline	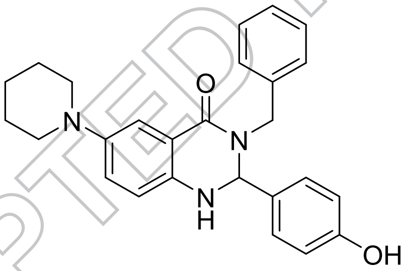	11	(Jiang, Yang, Wu, Guo, & You, 2011b)	Active
32	CK	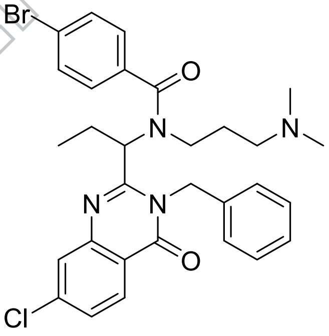	12	(Sakowicz et al., 2004)	Active

33	54	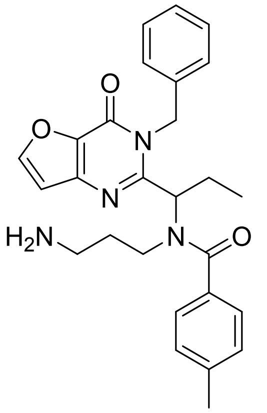	13	(Theoclitou et al., 2011)	Active
34	63	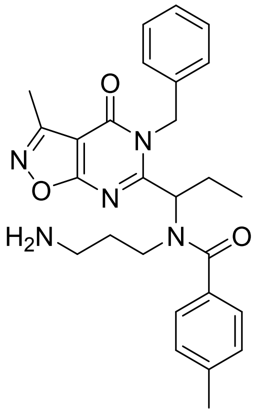	16	(Theoclitou et al., 2011)	Active
35	38	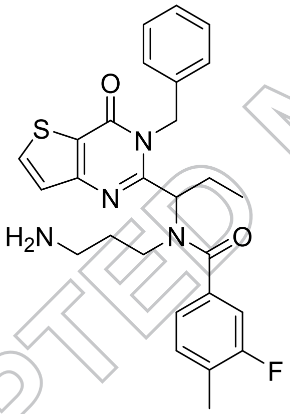	20	(Theoclitou et al., 2011)	Active
36	5	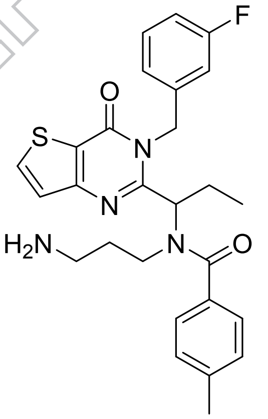	20	(Theoclitou et al., 2011)	Active

37	55	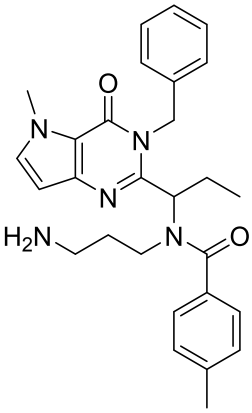	21	(Theoclitou et al., 2011)	Moderately active
38	10C	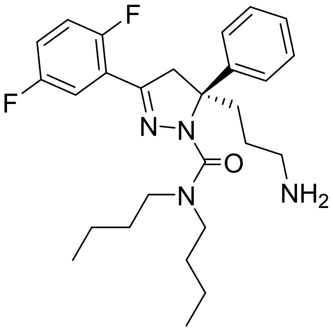	26	(Cox et al., 2006)	Moderately active
39	CPUYJ	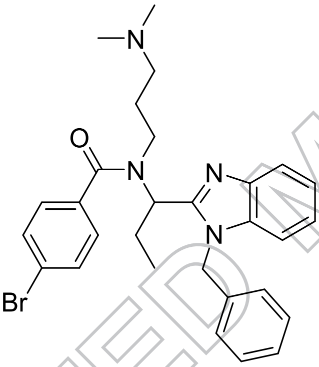	40	(Jiang, Yang, Wu, Guo, & You, 2011a)	Moderately active
40	BMCL	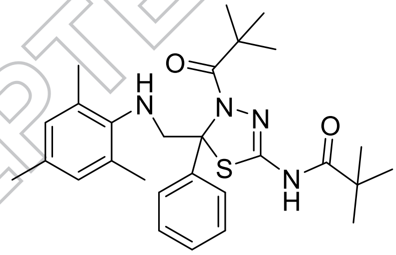	44	(Yamamoto et al., 2014)	Moderately active
41	8H	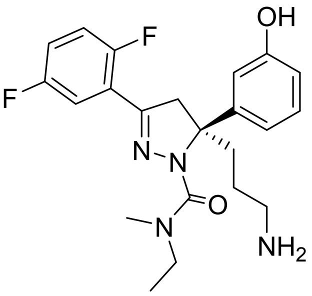	44	(Cox et al., 2006)	Moderately active

42	JMC	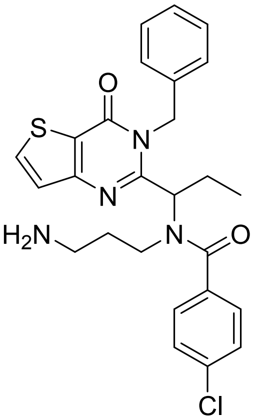	50	(Theoclitou et al., 2011)	Moderately active
43	10B	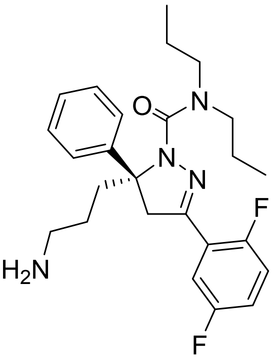	55	(Cox et al., 2006)	Moderately active
44	26	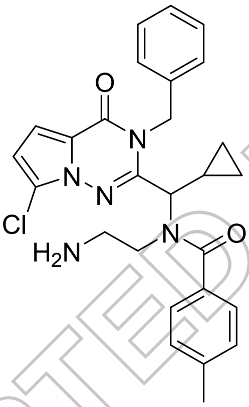	60	(Kim et al., 2006)	Moderately active
45	28	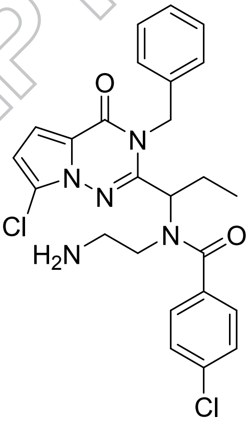	60	(Kim et al., 2006)	Moderately active

46	18	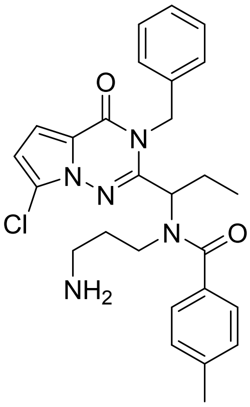	60	(Kim et al., 2006)	Moderately active
47	Pyrrolotriazineanalog	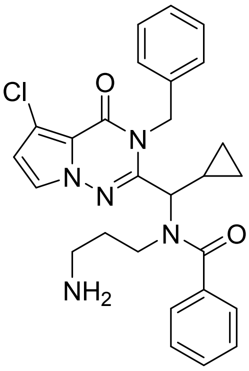	60	(Kim et al., 2006)	Moderately active
48	8I	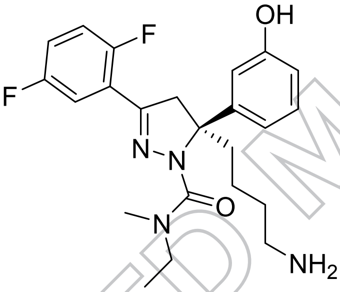	67	(Cox et al., 2006)	Moderately active
49	7	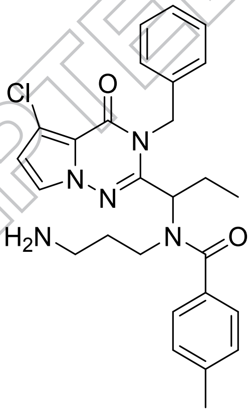	70	(Kim et al., 2006)	Moderately active

50	20	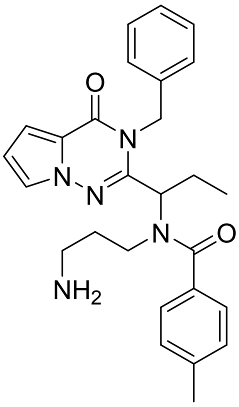	80	(Kim et al., 2006)	Moderately active
51	58	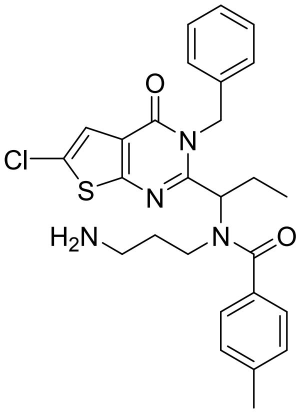 O N Cl S N H2N N O	85	(Theoclitou et al., 2011)	Moderately active
52	10D	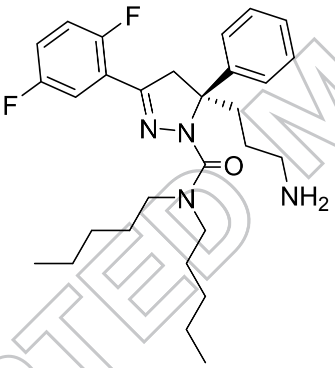	85	(Cox et al., 2006)	Moderately active
53	ARMC	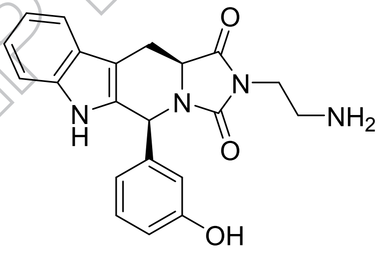 O N NH2 N H N O OH	90	(Hotha et al., 2003)	Moderately active

54	7	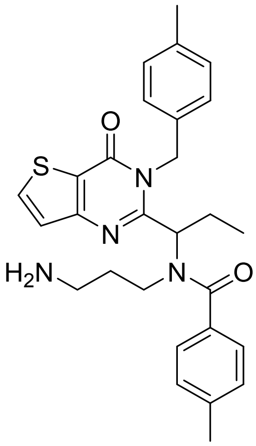	100	(Theoclitou et al., 2011)	Weakly active

Table S2CDOCKER energy and molecular interactions of bound ligand, training set ligands and top-ranked hits from each database

S. No.	Ligands	CDOCKER energy	Interactions after molecular docking		Interactions after molecular dynamics	
			Type of interactions (Distance in Å)	Key residues	Type of interactions (Distance in Å)	Key residues
1	SB-743921 (PDB ID: 4BXN)	-26.05	-NH: H-bond (2.81); -Cl: halogen (1.35)	Gly117 (O=C); Ala218 (-NH)	-----------	-----------
2	SB-743921 (**1**)	-26.05	-Cl: hydrophobic; -CH_3 of tolyl moiety: alkylinteractions	Leu214, Lys216; Leu132, Ala133	ring-C=O: H-bond (1.83); -CH_2: H-bond (2.50); NH_2:Salt bridge; π-Orbitals: hydrophobic; alkyl interactions	-NH:Arg104; O=C:Glu103; Asp115; Ala203, Pro122, Leu199, Leu125 and Val125
3	**2**	-32.63	-NH: H-bond (2.11); -N:C-H bond (2.92); -CH_3:C-H bond (2.73); π-Orbitals: hydrophobic; π-alkyl	Glu116 (O=C); Glu118; Glu116 (O=C); Glu118; Ala218	-----------	-----------

			interaction			
4	ARQ-621 (**3**)	-33.68	-NH$_2$: H-bond (2.78 and 1.83); -Methylene: C-H bond (2.76); -Methylene: C-H bond (2.92); π-Orbitals: hydrophobic; alkyl interactions; π-cation: electrostatic	Glu116 (O=C); Glu116 (O=C); Gly117; Leu214; Pro137 and Ala133; Arg119	-----------	-----------
5	AZD-4877 (**4**)	-33.47	-NH: H-bond (1.90); -Methylene: C-H bond (2.48); -Methylene: C-H bond (2.80); -Methylene: C-H bond (2.83); π-Orbitals: hydrophobic; alkyl interactions	Glu118 (O=C); Glu118 (O=C); Gly117; Glu118 (O=C); Ala218, Leu214 and Pro137; Pro137	-----------	-----------

6	MK-0731 (**5**)	-4.58	OH:H bond (2.20) -F: halogen (3.66, 2.77 and 3.05); -CH_3:C-H bond (2.46 and 2.99); π-Orbitals: hydrophobic	Arg119; Trp127,Glu118 and Gly117; Gly117 and Glu116; Ala218, Pro137 and Ala133	-----------	-----------
7	Filanesib (**6**)	-33.78	-F: halogen (2.79); -OCH_3:C-H bond (2.63 and 2.73); -NCH_3:C-H bond (2.59 and 2.90); π-Orbitals: hydrophobic; π-π stacking	Glu118 (O=C); Glu116 (O=C); Leu214; Pro137 and Ala133; Trp127	-----------	-----------
8	MB-41570 (Maybridge)	-42.70	-Ester CH_2: C-H bond (2.99); N-CH_3: C-H bond(2.89); π- sulphur; vdW interactions; alkyl	Glu116; Glu118; Tyr211; Ala133, Gly117, Ala218, Leu214, Glu128, and Phe144;	-Ester C=O: H bond (2.82); N-CH_3: C-H bond (2.59); π- sulphur; Piperazine CH_2: C-H bond (2.90); Ester methylene: C-H bond (2.73	Glu103; Lys192, Leu125, Trp122; Tyr196; Pro122; Glu103 and Trp112;

			interactions	Arg119 and Val210	& 2.65); alkyl interactions	Arg104 and Val195
9	CB-10358 (ChemBridge)	-39.19	-OCH$_3$: C-H bond (3.06); Piperidine-CH$_2$:C-H bond (2.85); π- π stacking; vdW interactions; π-alkyl interactions;	Glu116; Gly117 Tyr211; Trp127, Glu128, and Ala133; Leu214, Pro137, and Ala218	-CH$_2$: C-H bond (2.84); Piperidine-CH$_2$: C-H bond (3.00); -Ester CH$_3$: C-H bond (2.45); π- π stacking; π-alkyl interactions	O=C of Glu103 ; Gly102 Glu101; Try196; Ala203 and Leu199

Table S3 Top-ranked complex from each database and their fit values

S. No.	Ligand ID	Structure	CDOCKER energy (kcal/mol)	Fit value
1	CB-10358 (ChemBridge)	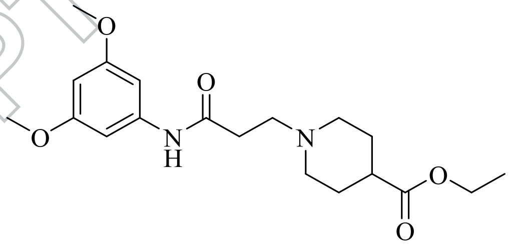	-39.19	3.12
2	MB-41570 (Maybridge)	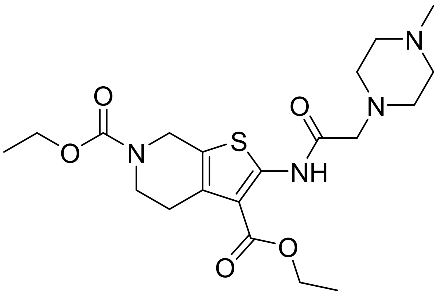	-42.70	3.28

References

Basso, A. D., Liu, M., Dai, C., Gray, K., Nale, L., Tevar, S., … Kirschmeier, P. (2010). SCH 2047069, a novel oral kinesin spindle protein inhibitor, shows single-agent antitumor activity and enhances the efficacy of chemotherapeutics. *Molecular Cancer Therapeutics*, *9*(11), 2993–3002. https://doi.org/10.1158/1535-7163.MCT-10-0548

Coleman, P. J., Schreier, J. D., Cox, C. D., Fraley, M. E., Garbaccio, R. M., Buser, C. A., … Hartman, G. D. (2007). Kinesin spindle protein (KSP) inhibitors. Part 6: Design and synthesis of 3,5-diaryl-4,5-dihydropyrazole amides as potent inhibitors of the mitotic kinesin KSP. *Bioorganic & Medicinal Chemistry Letters*, *17*(19), 5390–5395. https://doi.org/10.1016/j.bmcl.2007.07.046

Cox, C. D., Coleman, P. J., Breslin, M. J., Whitman, D. B., Garbaccio, R. M., Fraley, M. E., … Hartman, G. D. (2008). Kinesin spindle Protein (KSP) inhibitors. 9. Discovery of (2*S*)-4-(2,5-difluorophenyl)-*N*-[(3*R*,4*S*)-3-fluoro-1-methylpiperidin-4-yl]-2-(hydroxymethyl)-*N*-methyl-2-phenyl-2,5-dihydro-1*H*-pyrrole-1-carboxamide (MK-0731) for the treatment of taxane-refractory cancer. *Journal of Medicinal Chemistry*, *51*(14), 4239–4252. https://doi.org/10.1021/jm800386y

Cox, C. D., Torrent, M., Breslin, M. J., Mariano, B. J., Whitman, D. B., Coleman, P. J., … Hartman, G. D. (2006). Kinesin spindle protein (KSP) inhibitors. Part 4: Structure-based design of 5-alkylamino-3,5-diaryl-4,5-dihydropyrazoles as potent, water-soluble inhibitors of the mitotic kinesin KSP. *Bioorganic & Medicinal Chemistry Letters*, *16*(12), 3175–3179. https://doi.org/10.1016/j.bmcl.2006.03.040

Davis, D. A., Sarkar, S. H., Hussain, M., Li, Y., & Sarkar, F. H. (2006). Increased therapeutic potential of an experimental anti-mitotic inhibitor SB715992 by genistein in PC-3 human prostate cancer cell line. *BMC Cancer*, *6*(1), 22. https://doi.org/10.1186/1471-2407-6-22

Garbaccio, R. M., Fraley, M. E., Tasber, E. S., Olson, C. M., Hoffman, W. F., Arrington, K. L., … Hartman, G. D. (2006). Kinesin spindle protein (KSP) inhibitors. Part 3: Synthesis and evaluation of phenolic 2,4-diaryl-2,5-dihydropyrroles with reduced hERG binding and employment of a phosphate prodrug strategy for aqueous solubility. *Bioorganic & Medicinal Chemistry Letters*, *16*(7), 1780–1783. https://doi.org/10.1016/j.bmcl.2005.12.094

Garbaccio, R. M., Tasber, E. S., Neilson, L. A., Coleman, P. J., Fraley, M. E., Olson, C., …

Hartman, G. D. (2007). Kinesin spindle protein (KSP) inhibitors. Part 7: Design and synthesis of 3,3-disubstituted dihydropyrazolobenzoxazines as potent inhibitors of the mitotic kinesin KSP. *Bioorganic and Medicinal Chemistry Letters*, *17*(20), 5671–5676. https://doi.org/10.1016/j.bmcl.2007.07.067

Hotha, S., Yarrow, J. C., Yang, J. G., Garrett, S., Renduchintala, K. V, Mayer, T. U., & Kapoor, T. M. (2003). HR22C16: a potent small-molecule probe for the dynamics of cell division. *Angewandte Chemie (International Ed. in English)*, *42*(21), 2379–82. https://doi.org/10.1002/anie.200351173

Jiang, C., Yang, L., Wu, W.-T., Guo, Q.-L., & You, Q.-D. (2011a). CPUYJ039, a newly synthesized benzimidazole-based compound, is proved to be a novel inducer of apoptosis in HCT116 cells with potent KSP inhibitory activity. *The Journal of Pharmacy and Pharmacology*, *63*(11), 1462–9. https://doi.org/10.1111/j.2042-7158.2011.01350.x

Jiang, C., Yang, L., Wu, W.-T., Guo, Q.-L., & You, Q.-D. (2011b). De novo design, synthesis and biological evaluation of 1,4-dihydroquinolin-4-ones and 1,2,3,4-tetrahydroquinazolin-4-ones as potent kinesin spindle protein (KSP) inhibitors. *Bioorganic & Medicinal Chemistry*, *19*(18), 5612–5627. https://doi.org/10.1016/j.bmc.2011.07.029

Kim, K. S., Lu, S., Cornelius, L. A., Lombardo, L. J., Borzilleri, R. M., Schroeder, G. M., … Roussell, D. L. (2006). Synthesis and SAR of pyrrolotriazine-4-one based Eg5 inhibitors. *Bioorganic & Medicinal Chemistry Letters*, *16*(15), 3937–3942. https://doi.org/10.1016/j.bmcl.2006.05.037

Sakowicz, R., Finer, J. T., Beraud, C., Crompton, A., Lewis, E., Fritsch, A., … Wood, K. W. (2004). Antitumor Activity of a Kinesin Inhibitor. *Cancer Research*, *64*(9), 3276–3280.

Schiemann, K., Finsinger, D., Zenke, F., Amendt, C., Knöchel, T., Bruge, D., … Anzali, S. (2010). The discovery and optimization of hexahydro-2H-pyrano[3,2-*c*]quinolines (HHPQs) as potent and selective inhibitors of the mitotic kinesin-5. *Bioorganic and Medicinal Chemistry Letters*, *20*(5), 1491–1495. https://doi.org/10.1016/j.bmcl.2010.01.110

Theoclitou, M., Aquila, B., Block, M. H., Brassil, P. J., Castriotta, L., Code, E., … Zheng, X. (2011). Discovery of (+)-*N*-(3-aminopropyl)-*N*-[1-(5-benzyl-3-methyl-4-oxo-[1,2]thiazolo[5,4-*d*]pyrimidin-6-yl)-2-methylpropyl]-4-methylbenzamide (AZD4877), a kinesin spindle protein inhibitor and potential anticancer agent. *Journal of Medicinal Chemistry*, *54*(19), 6734–50. https://doi.org/10.1021/jm200629m

Verschraegen, C., Cohen, R. B., Olszanski, A. J., Shaheen, M., Nishida, Y., Bauman, J., … Westin, E. H. (2014). Abstract A86: A phase 1 study of LY2523355, an Eg5 inhibitor, administered on Days 1, 2, and 3 with or without pegfilgrastim in patients with advanced malignancy (NCT01214629). *Molecular Cancer Therapeutics*, *10*(11 Supplement), A86 LP-A86. Retrieved from http://mct.aacrjournals.org/content/10/11_Supplement/A86.abstract

Yamamoto, J., Amishiro, N., Kato, K., Ohta, Y., Ino, Y., Araki, M., … Murakata, C. (2014). Synthetic studies on mitotic kinesin Eg5 inhibitors: Synthesis and structure–activity relationships of novel 2,4,5-substituted-1,3,4-thiadiazoline derivatives. *Bioorganic & Medicinal Chemistry Letters*, *24*(16), 3961–3963. https://doi.org/10.1016/j.bmcl.2014.06.034

ANUSCRIPT

Spectral characterization of the hits (Maybridge and ChemBridge)

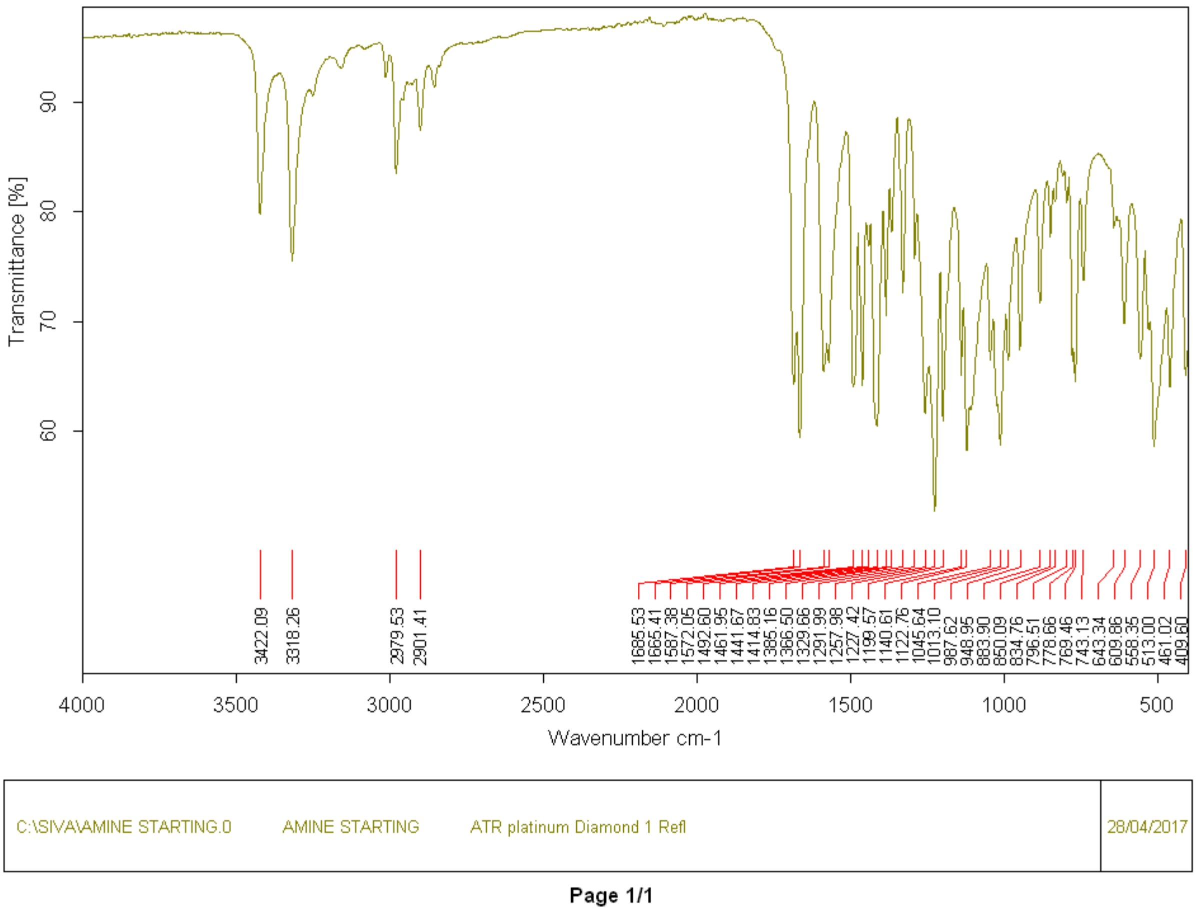

Figure S1 FT-IR spectrum of starting compound **3**

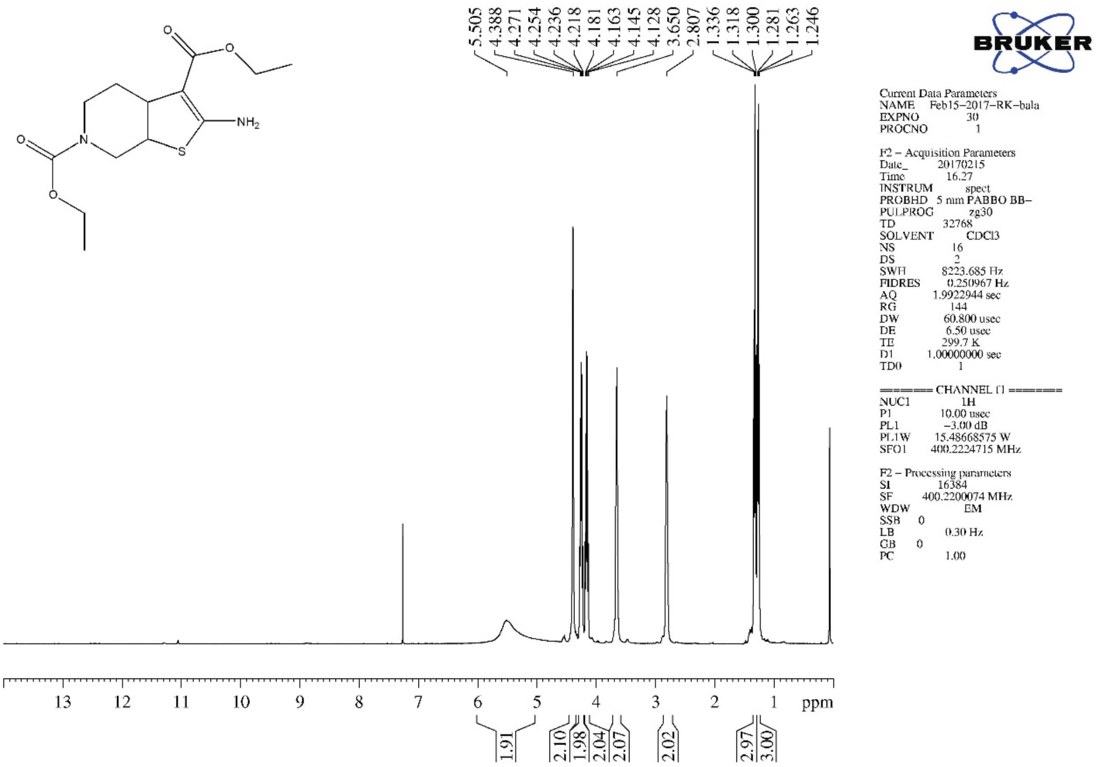

Figure S2 ^{1}H NMR of compound **3**

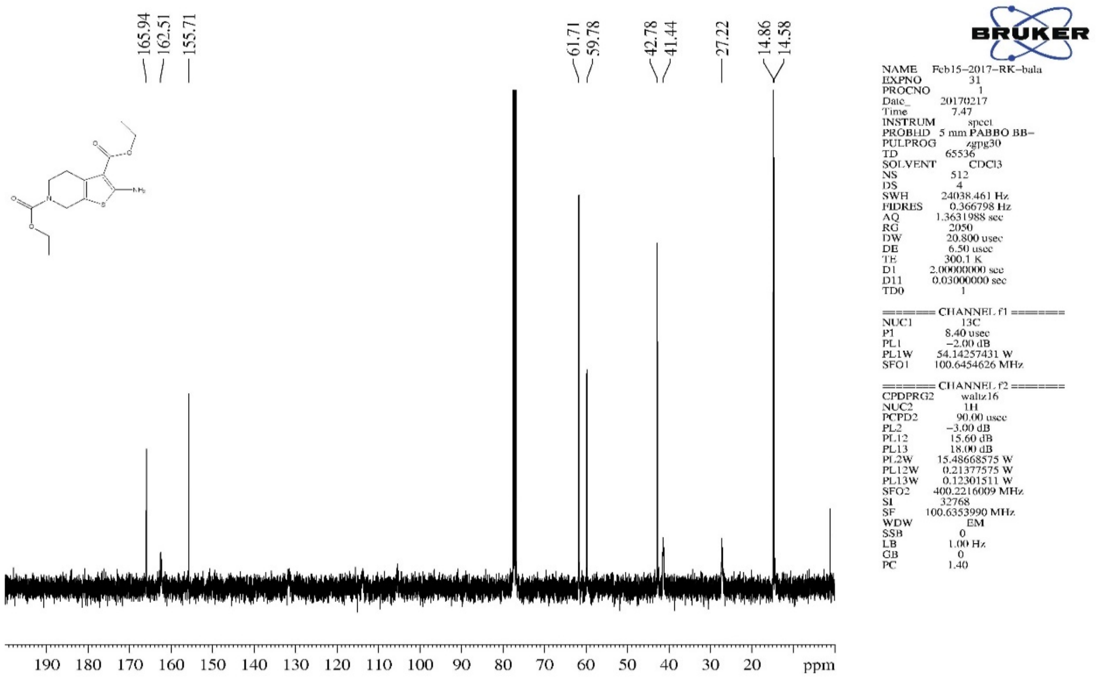

Figure S3 ^{13}C NMR of compound **3**

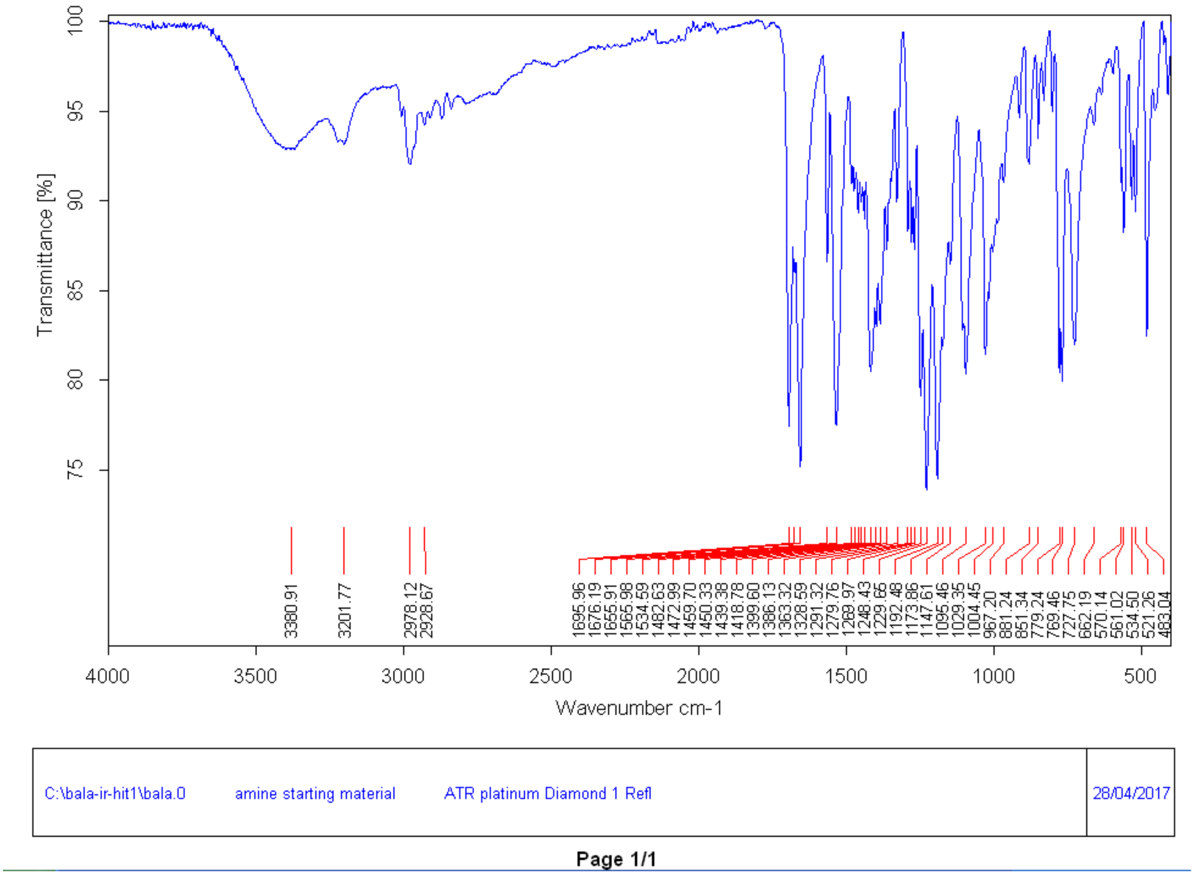

Figure S4 FT-IR spectrum of compound **4**

ACCEPTED

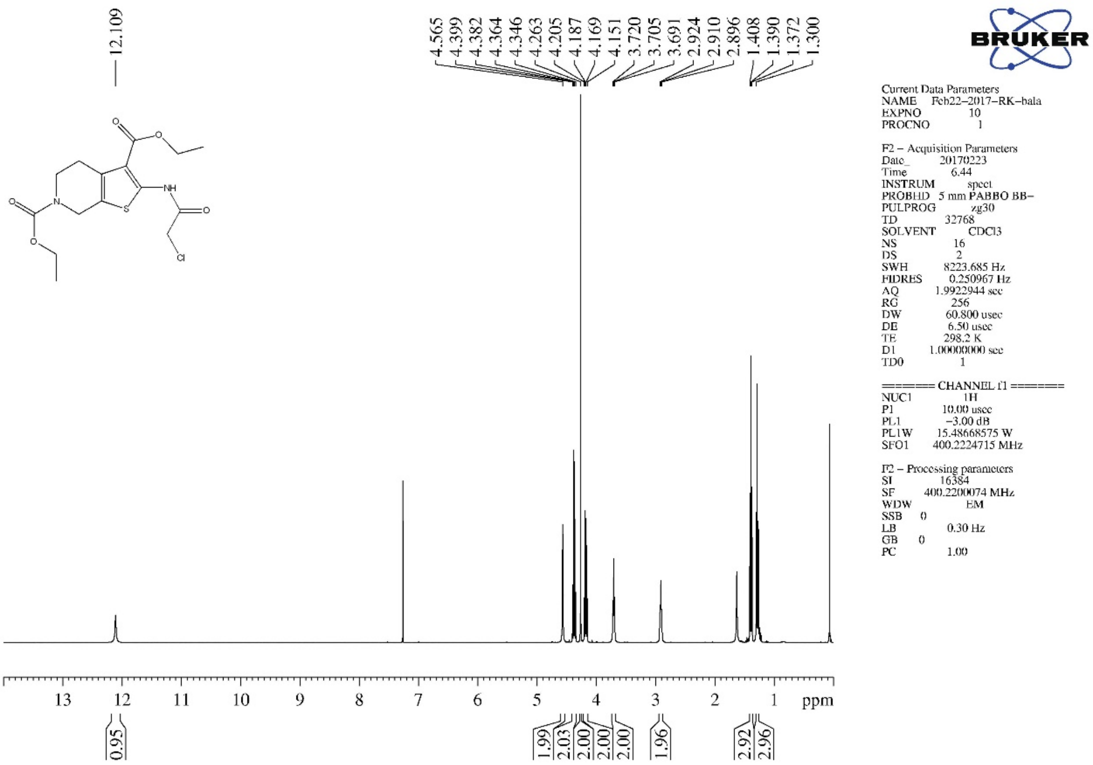

Figure S5 ^{1}H NMR of compound **4**

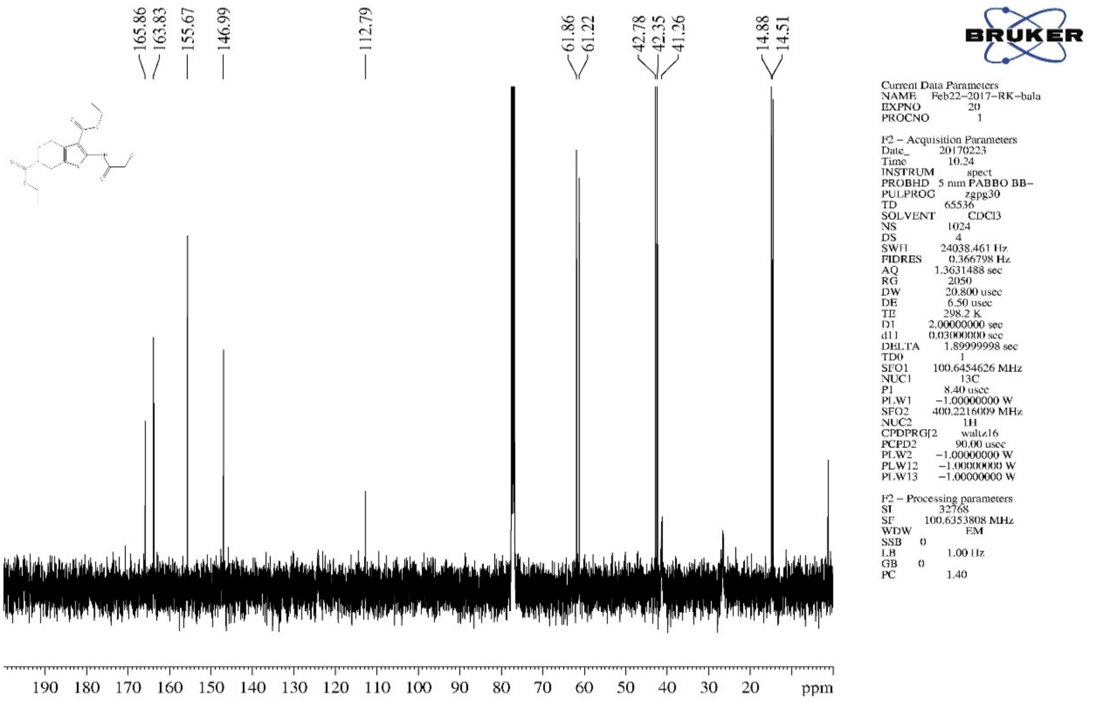

Figure S6 ^{13}C NMR of compound **4**

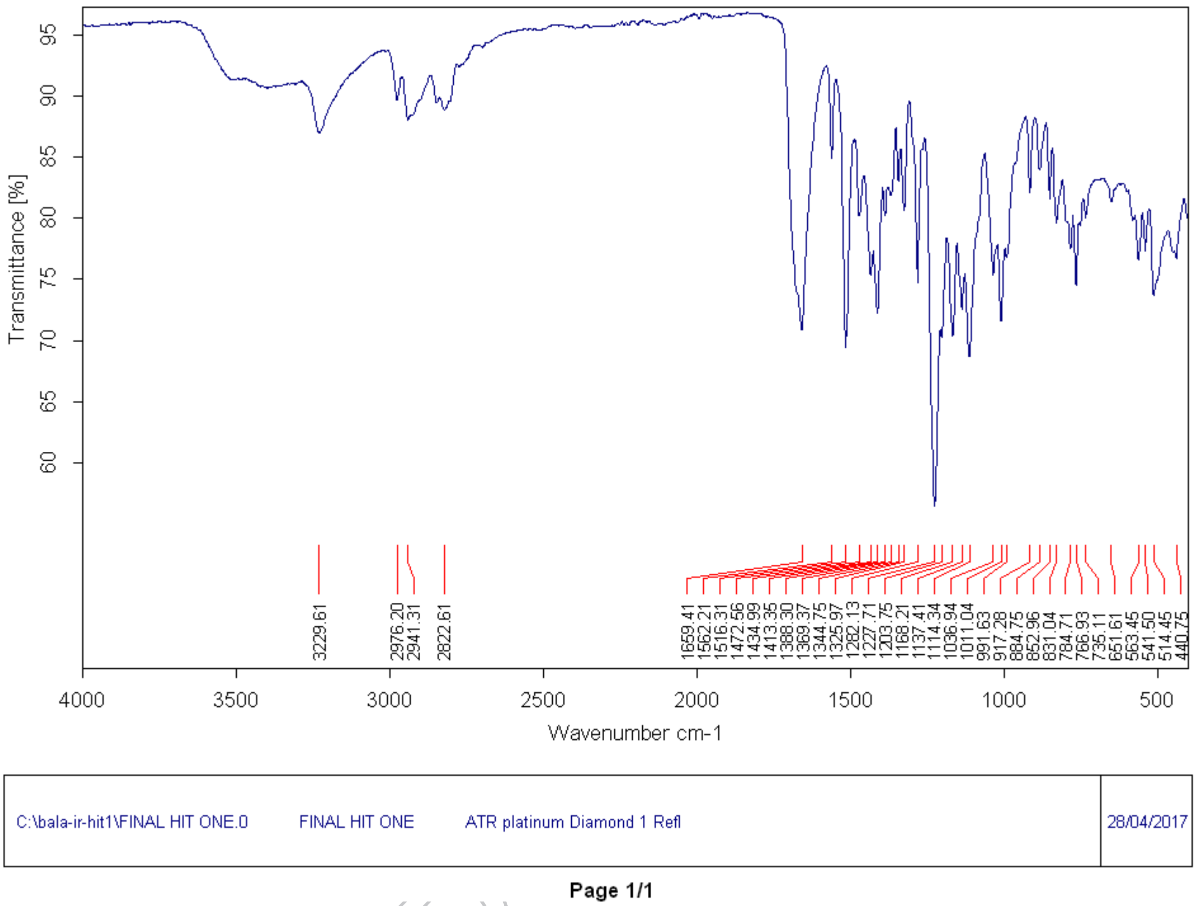

Figure S7 FT-IR spectrum of compound **5 (Maybridge hit)**

ACCEPTED

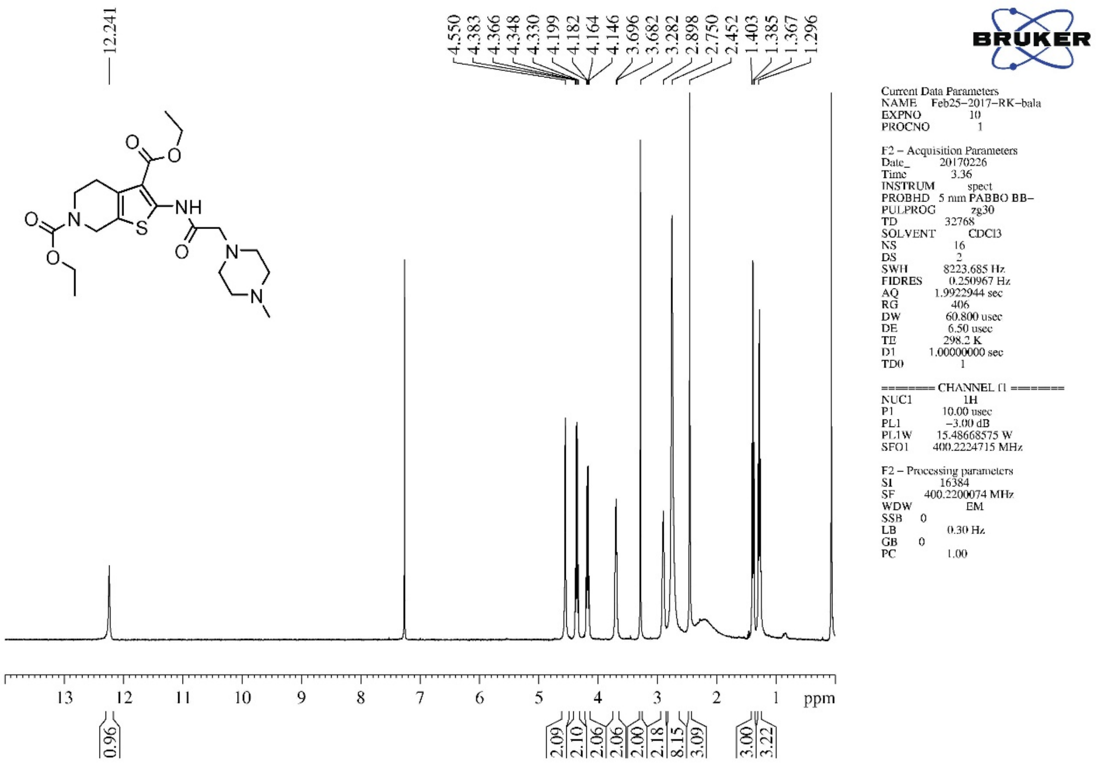

Figure S8 ^{1}H NMR of compound **5 (Maybridge hit)**

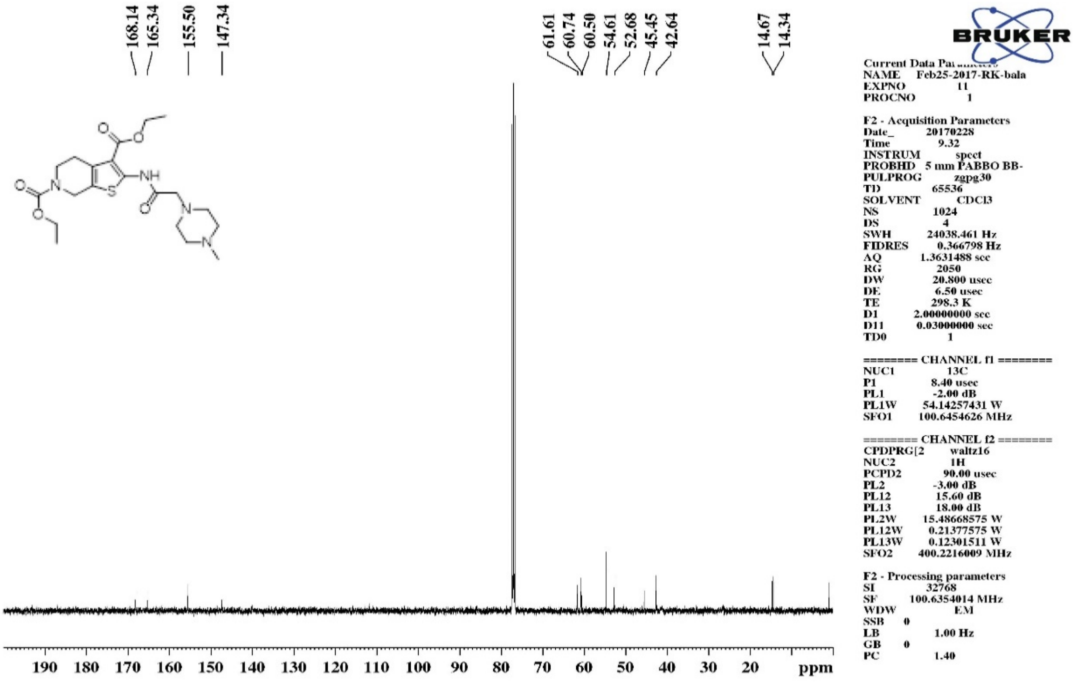

Figure S9 ^{13}C NMR of compound **5 (Maybridge hit)**

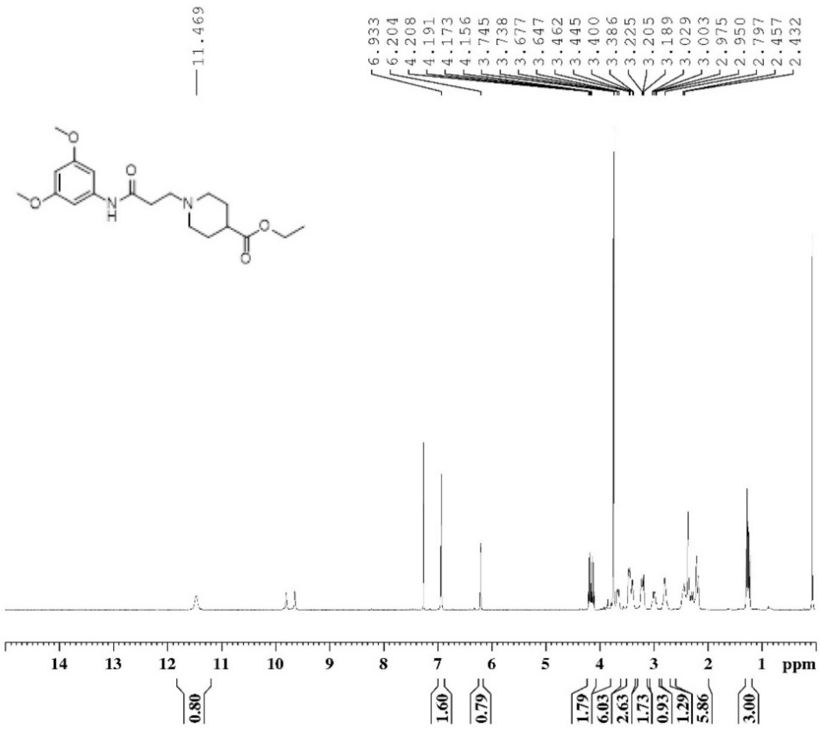

```
Current Data Parameters
NAME     Apr28-2017-RK-bala
EXPNO              20
PROCNO              1

F2 - Acquisition Parameters
Date_        20170428
Time            19.25
INSTRUM          spect
PROBHD   5 mm PABBO BB-
PULPROG          zg30
TD              32768
SOLVENT          CDCl3
NS                 16
DS                  2
SWH          8223.685 Hz
FIDRES       0.250967 Hz
AQ          1.9922944 sec
RG                362
DW             60.800 usec
DE               6.50 usec
TE              298.2 K
D1         1.00000000 sec
TD0                 1

======== CHANNEL f1 ========
NUC1               1H
P1              10.00 usec
PL1             -3.00 dB
PL1W      15.48668575 W
SFO1      400.2224715 MHz

F2 - Processing parameters
SI              16384
SF        400.2200076 MHz
WDW                EM
SSB      0
LB               0.30 Hz
GB       0
PC               1.00
```

Figure S10 ^{1}H NMR spectrum of **ChemBridge hit**

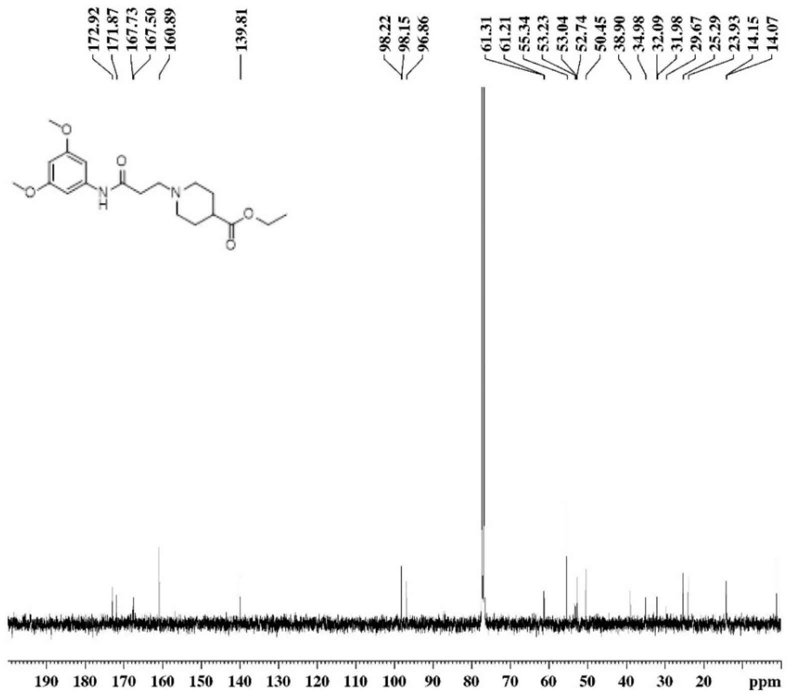

```
Current Data Parameters
NAME     Apr29-2017-RK-bala
EXPNO              30
PROCNO              1

F2 - Acquisition Parameters
Date_        20170430
Time             5.17
INSTRUM          spect
PROBHD   5 mm PABBO BB-
PULPROG        zgpg30
TD              65536
SOLVENT          CDCl3
NS               1024
DS                  4
SWH         24038.461 Hz
FIDRES       0.366798 Hz
AQ          1.3631488 sec
RG               2050
DW             20.800 usec
DE               6.50 usec
TE              298.2 K
D1         2.00000000 sec
D11        0.03000000 sec
TD0                 1

======== CHANNEL f1 ========
NUC1              13C
P1               8.40 usec
PL1             -2.00 dB
PL1W      54.14257431 W
SFO1      100.6454626 MHz

======== CHANNEL f2 ========
CPDPRG[2       waltz16
NUC2               1H
PCPD2           90.00 usec
PL2             -3.00 dB
PL12            15.60 dB
PL13            18.00 dB
PL2W      15.48668575 W
PL12W      0.21377575 W
PL13W      0.12301511 W
SFO2      400.2216009 MHz

F2 - Processing parameters
SI              32768
SF        100.6354014 MHz
WDW                EM
SSB      0
LB               1.00 Hz
GB       0
PC               1.40
```

Figure S11 ^{13}C NMR spectrum of**ChemBridge hit**

KSP ATPase inhibition profiles of Hits

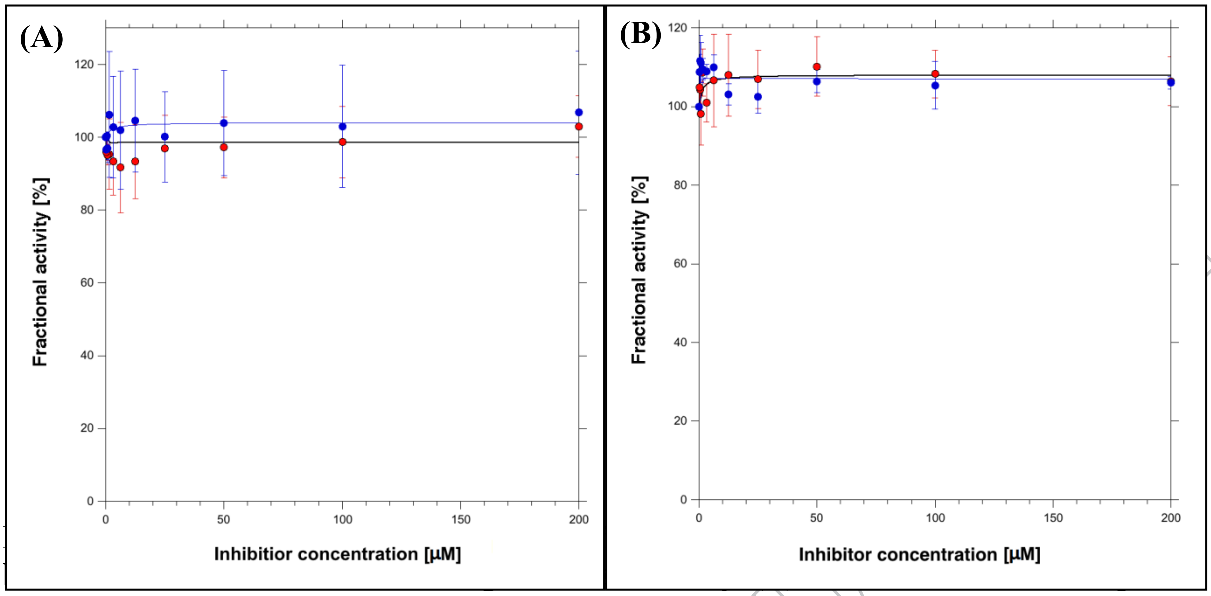

ATPase activity in the presence of increasing Maybridge hit (red dots) and ChemBridge hit (blue dots) concentrations. **(B)** Inhibition of the MT-stimulated Eg5 ATPase activities in the presence of increasing Maybridge hit (red dots) and ChemBridge hit (blue dots) concentrations. The results indicate that both the hits have no inhibition effect on neither the basal nor the MT-stimulated Eg5 ATPase activities. The data points were fitted using Kaleidagraph 4.0. All measurements were performed in triplicate.